Dynamic physiology broadens the molecular composition of kelp-derived dissolved organic matter exported to the coastal ocean

Chance J. English[1,2,3*], *Tilman Schramm*[3], *Keri Opalk*[1], *Dave A. Siegel*[2], *Daniel Petras*[3], *Craig A. Carlson*[1,4]

1. Marine Science Institute/Department of Ecology, Evolution and Marine Biology, University of California Santa Barbara, CA, USA
2. Earth Research Institute, University of California, Santa Barbara, CA 93106
3. Department of Biochemistry, University of California, Riverside, California, USA
4. Bermuda Institute of Ocean Sciences, a unit of the Julie Ann Wrigley Global Futures Laboratory at Arizona State University, St. George's, Bermuda

* Corresponding author: Chance J. English
Email: **chance.english@ucr.edu**
(951) 286-8416

Key Words: macroalgae, kelp, dissolved organic matter, metabolomics, organic halogens, recalcitrant, sequestration

Author Contribution Statement

CJE and CAC conceptualized the research. CJE collected material for and ran the incubations. CJE, TS, and KO collected data and performed laboratory measurements. CJE, TS, KO, DP, DAS, & CAC contributed to interpreting the results and writing/editing the manuscript. CAC, DAS, and DP acquired funding for the research.

CJE: chance.english@ucr.edu

TS: tschr009@ucr.edu

KO: keri.opalk@ucsb.edu

DAS: davey@eri.ucsb.edu

DP: dpetras@ucr.edu

CAC: craig.carlson@bios.asu.edu

Abstract

Metabolites are exuded by marine primary producers and contribute to the pool of dissolved organic matter that structures the ecology and biogeochemistry of marine ecosystems. In the coastal ocean, macroalgae such as kelps fix inorganic carbon via photosynthesis and release a fraction of that carbon as dissolved organic matter. In this study, we characterized the exo-metabolome of the globally distributed foundation species *Macrocystis pyrifera* (giant kelp) using liquid chromatography-tandem mass spectrometry. We assessed the exuded metabolites across gradients in giant kelp physiological state and productivity driven by seasonal, environmental, and intrinsic age-dependent biological factors. Our results showed that kelp physiological condition is a main driver of exudate composition, as revealed by changes in the exudate stoichiometry and the relative abundance of molecular families. Notably, we identified that giant kelp may be an important source of brominated dissolved organic matter to the coastal ocean during senescence, with exudate bromine to carbon molar ratios (Br:C) reaching 0.14. Lastly, we found that roughly 20% of giant kelp dissolved organic carbon is recalcitrant to microbial remineralization. Surprisingly, we found no significant variability in this recalcitrance across giant kelp physiology, despite large shifts in its DOM composition. This suggests that a diverse mixture of kelp-derived metabolites, including peptides, brominated phenols, and eicosanoids, may contribute to long-term carbon storage.

1. Introduction

Macroalgae are the foundation for many critical marine habitats and exhibit significant biomass along the world's coastlines[1,2]. This biomass is dominated by kelp forests which have been suggested to play a major role in marine carbon sequestration due to their rapid growth rates, efficient carbon export, and high carbon content[3]. As a result, large-scale seaweed aquaculture and restoration are considered mitigation strategies for marine carbon dioxide removal[4–6]. In natural macroalgal systems, this sequestration potential is proposed to be dominated by the production of recalcitrant dissolved organic matter (DOM)[6,7]. however, we lack basic data regarding its composition, production, and decomposition. Constraining the latter is particularly important, as it controls the contribution of macroalgae to carbon sequestration, but is reported to range from 7 – 86% of released dissolved organic carbon (DOC)[8–10]. Before large-scale macroalgae aquaculture or restoration can be verified as a marine carbon dioxide removal (mCDR) strategy, the reactivity of the kelp carbon produced and the controls on its variability must be evaluated.

A key regulator of DOM decomposition rates is its molecular composition[11,12]. Although the chemical composition of kelps has been explored extensively for the discovery of desirable natural products for industrial, nutritional, or pharmaceutical applications, this has largely focused on the compounds found within the kelp tissue rather than exuded material (i.e. the exo-metabolome)[13–18]. Previous work explored the exo-metabolome of macroalgae, such as *Dictyota*[19] and *Sargassum*[20], using high-resolution mass spectrometry, but these studies had limited sampling resolution and did not consider the effects of environmental conditions or physiology of the organism. In

contrast, the studies that considered seasonal and physiological gradients on kelp exudate composition used only coarse chemical characterization or focused on targeted compounds or compound classes[21–23]; thus, there is a lack of high-resolution kelp-derived DOM characterization across gradients in kelp physiology. To improve understanding of macroalgae in long-term carbon storage, we need explore the composition and recalcitrance of the DOM from kelps (Class Phaeophyceae; order Laminariales), which dominate global macroalgal net primary production[1,24], make up more than 40% of global macroalgae aquaculture[25], and are candidates for large-scale cultivation for mCDR.

It is well established that the exo-metabolome of primary producers is dynamic and responds to nutrient stress, pathogens, and/or the developmental stage of the organism[26–28]. Likewise, the composition of DOM derived from kelps should be studied across the same gradients. For temperate kelp forests, physiology and growth rates are governed by seasonal gradients in temperature, nitrate concentrations, and light, as well as intrinsic biological factors such as senescence[22,29,30]. Senescence, an age-related decline in physiological condition, has been shown to be particularly important, as kelp senescence resulted in elevated DOM production rates[31,32]. Therefore, a major motivation of this study was to characterize the exo-metabolome of kelp from the mature growing phase to senescence.

Describing the composition of DOM released from primary producers is critical to understanding their biogeochemical and ecological role in ecosystems[19,27,33]. This is challenging, as marine DOM consists of thousands of unique molecules, and the low representation of reference compounds impedes characterization. Despite these

limitations, advances in untargeted metabolomics and molecular networking can be applied to semi quantitatively measure the elemental and compound class level composition of highly complex marine DOM samples[34–38]. These techniques enable comparative metabolomics, allowing us to observe the composition of kelp-derived DOM across environmental and biological gradients. By identifying compounds that are unique to these conditions, we can begin to understand the factors contributing to kelp's adaptation to environmental stress and the potential impacts to marine biogeochemistry.

In this study, we examined the composition of DOM produced by the canopy-forming kelp *Macrocystis pyrifera*, hereafter giant kelp. Giant kelp is a globally distributed foundation species and an ideal model for investigating the environmental and physiological controls on exuded DOM composition. It's continuous growth and predictable age-dependent senescence enable the examination of these processes across large gradients in seawater temperature, nutrient concentrations, and developmental stage[30]. By combining high temporal resolution sampling of giant kelp across seasons and developmental stages with untargeted liquid chromatography tandem mass spectrometry (LC-MS/MS), we assessed the diversity and recalcitrant nature of kelp-derived DOM across gradients in its physiology.

2. Materials and Methods

2.1 Environmental and physiological parameters, kelp sampling and incubation framework

The metabolomics data presented here complement previously reported background environmental, physiological, and microbiome data reported in English et

al., (2025)[31] & English et al., (2025)[39]. Giant kelp blades were sampled from Mohawk Reef (34.3941°N, 119.7296° W) in Santa Barbara, California USA, between August 2023 and June 2024. *In situ* seawater temperature was measured by a mooring maintained by the Santa Barbara Coastal Long-Term Ecological Research (SBC-LTER) program[40]. Daily nitrate concentrations were estimated from temperature using a temperature-to-nitrate (T2N) relationship[41]. The T2N model was fit using a generalized additive model (R package *mgcv*[42]) of temperature and measured nitrate data sampled from Mohawk Reef between 2006 - 2024. T2N-estimated nitrate concentrations were compared to measured nitrate concentrations collected monthly by the SBC-LTER at Mohawk Reef[43].

Samples for DOC and metabolites produced by giant kelp were collected from the incubations of individual kelp blades sampled from tagged cohorts. Tagged cohorts of blades were established in the nitrate-depleted summer and nitrate replete-spring. From both cohorts, six blades were sampled from unique kelp fronds every two to three weeks across the mature (< 50 days of age) and senescent (> 50 days of age) periods of giant kelp development. Blades were transported in ambient seawater to a near-shore laboratory and incubated for 24 hours in 5 L of 0.2 µm filter sterilized seawater collected from near-shore and maintained at *in situ* temperatures (13 – 19 ºC) with a 12-hour light: dark cycle. At the beginning and end of the incubation, 500 ml of incubation media was sampled for DOC and dissolved inorganic carbon (DIC), and 1 L was sampled for dissolved metabolites.

Kelp physiology was measured post-incubation as the tissue chlorophyll *a* to carbon (Chl:C) and carbon to nitrogen (C:N) ratios[44]. Briefly, chlorophyll a was extracted

154 from a 0.8 cm^2 punch from the kelp tissue with a two-step liquid phase extraction with
155 DMSO and a 3:1:1 solution of acetone, methanol, and water. The extract's absorbance
156 between 350 – 800 nm was measured on a Shimadzu UV 2401PC (Tokyo, Japan) and
157 converted to chlorophyll *a* concentration using a known equation[45]. For tissue C:N
158 analysis, blades were dried at 60 ºC for three days, ground to a fine powder and
159 analyzed on a CE-440 CHN/O/S elemental analyzer (Exeter Analytical, Exeter, UK).
160
161 *2.2 Maximum photosynthetic rate (P_{max})*
162 P_{max} was measured as DIC drawdown in the incubation seawater when kelp
163 blades were incubated at saturating irradiances (> 300 µmol photons m^{-2} s^{-1}). Samples
164 of incubation seawater were collected by siphon into 125 ml serum bottle and preserved
165 with a solution (10% w/v) of $HgCl_2$ (0.1% v/v final concentration). DIC samples were
166 analyzed with an inorganic carbon analyzer (AIRICA by MARIANDA, Kiel, Germany)[36]
167 and calibrated against certified reference material (CRM Batch #206 & #216; Dickson
168 Lab, San Diego, USA). Rates of P_{max} were calculated as:
169 $$P_{max}\ (\mu mol\ C\ g_{DW}\ hr^{-1}) = \frac{[DIC]_0 - [DIC]_t * V}{T * m} \quad (1)$$
170 where $[DIC]_0$ and $[DIC]_t$ are the DIC concentrations (µM C) at the beginning and end of
171 each incubation, respectively. V is the volume of seawater during the incubation, T is
172 the incubation time, and m is the tissue dry weight.
173
174 *2.3 DOM solid-phase extraction, mass spectral data analysis, molecular formula and*
175 *compounds class annotations, and molecular networking*

For metabolomics, 1 L of incubation and ambient seawater (i.e. seawater before incubation with kelp) were filtered through pre-combusted 0.3 µm GF-75 filteres, acidified to pH ~2 with Optima® HCl (Fisher Scientific) and DOM was extracted by solid-phase extraction (SPE) with 1g Priority PolLutant (PPL) cartridges (Bond Elut, Agilent) following Petras et al.[34]. With the exception of sampling on 5/7/24 and 5/28/24 in the spring, we sampled the exo-metabolites from six kelp blades and one ambient seawater control. Regarding those specific dates, we had enough PPL columns available to support sampling of three kelp samples and the ambient control on 5/7/24, but were unable to sample for metabolites on 5/28/24. PPL columns were resupplied in time for regular sampling at the end of the spring cohort on 6/16/24. Concentrated samples were desalted with 3 bed volumes of pH ~ 2 LC-MS water and then dried under vacuum for 5 minutes. DOM was eluted from the columns with 6 mL of 100% methanol (LC-MS grade), dried using high-purity nitrogen and resuspended in 1 mL of 80% LC-MS grade methanol with 1% formic acid. Process blanks (n = 3) were generated using the same workflow with LC-MS grade water.

Samples were analyzed on a Vanquish ultra-high performance liquid chromatography system (UHPLC) coupled to an Exploris 480 Orbitrap Mass Spectrometer (Thermo Fisher Scientific). Chromatographic separation was performed with a C18 column (Kinetex, 150 x 2 mm, 1.8 µm particle size, 100 Å pore size, Phenomenex, Torrance, USA) with a flowrate of 0.5 mL min^{-1} (Solvent A: H2O + 0.1% formic acid (FA), Solvent B: Acetonitrile + 0.1% FA). After injection, the samples were eluted over a 10 minute gradient, including 30 seconds of 5% Solvent B, across a linear gradient over 7.5 minutes of 5 to 50% Solvent B and 2 minutes 50 to 99% Solvent B,

followed by a 2 minute washout at 99% B and a 3 minute reequilibration phase at 5% B; ion data was collected through the washout phase. LC-MS grade methanol blank injections were conducted every 5 samples to control for carry over. Mass and retention time accuracy and drift were monitored with a quality control (QC) mix of six standard compounds (sulfamethazine, sulfamethizole, sulfachloropyridazine, sulfadimethoxine, amitryptiline, coumarin-314).

Data-dependent acquisition (DDA) of tandem mass spectrometry (MS/MS) spectra was performed in positive and negative ionization modes. The parameters for each mode were identical except for switching the polarity. Electrospray ionization (ESI) parameters were set to 50 AU for sheath gas flow, 12 AU for auxiliary, and 1 AU for sweep gas. The auxiliary gas 15 temperature was 400°C. The spray voltage was set to 3.0 kV (ESI+) and -2.5 kV (ESI-) with the inlet capillary at 250°C. Additionally, a 50 V S-lens was applied. For the full scan (MS1) acquisition, the scan range was 150–1,500 m/z with a resolution at m/z 200 (Rm/z 200) of 120,000 with one micro-scan. Automated gain control (AGC) was set to 1.0E6 with a maximum ion injection time of 100 milliseconds. In addition to MS1 survey, a maximum of 5 MS/MS scans of the most abundant ions per duty cycle were measured with Rm/z 200 of 15,000 with one micro-scan. Automatic gain control targets were set to 5.0E5 with a minimum 10% C-trap filling for MS/MS. MS/MS precursor selection windows were set to m/z 1. The normalized collision energy was increased from 25 to 35 to 45%, with z = 1 as the default charge state. MS/MS scans were triggered at the apex of chromatogram peaks within 2-15 seconds of their first occurrence. Dynamic exclusion was set to 5 seconds. Ions with unassigned charge states were excluded from DDA and isotope peaks.

To check for mass to charge (m/z) and retention time stability, the standard compound samples were first analyzed as a quality control check (Figures S1 and S2). All raw and processed LC-MS/MS data as well as processed MS/MS files are available through the Mass Spectrometry Interactive Virtual Environment (MassIVE) repository (massive.ucsd.edu) with accession number MSV000095805. Following QC, raw .ms files were converted to .mzML and feature identification was carried out using mzmine (v 4.7.8)[36]. Mass detection was performed in centroid mode with a noise threshold level of 1.0E05 for MS1 and 1.0E03 for MS2. Chromatograms were built with a minimum peak height of 3.0E05, a minimum timespan of 0.02 minutes, and a relative mass tolerance of 10 ppm. Chromatographic resolution was performed with the baseline cutoff algorithm with a baseline level of 1.0E05 and a minimum height of 5.0E05 and peak duration range of 0.01 to 2.0 minutes. For isotope peak grouping, m/z and retention time tolerances were set to 10 ppm and 0.1 min, respectively, and a maximum charge of 2 was allowed. The most intense peak was selected as the monoisotopic ion. We applied the following thresholds to align extracted ion chromatograms (XICs) between samples: 0.015-min retention time tolerance with 25% weighting and 10-ppm mass tolerance with 75% weighting. After alignment, the peak list filtering option was used to select XICs that contained at least two isotope peaks and that occurred at least twice across all samples and had an MS2 scan. The aligned peak list was further filtered to remove as duplicates any XICs within 5-ppm mass windows and 0.1-min retention time windows. After filtering, gaps in the feature matrix were filled with the original peak information using the multithreaded peak finder algorithm with a 10-ppm mass tolerance and 0.1 min retention time tolerance. Consensus MS/MS spectra were

exported as .mgf files and submitted for feature-based molecular networking in the GNPS2 environment and compared against the GNPS and National Institute of Standards and Technology (NIST) 2020 mass spectral library. Features were connected in molecular networks if they had high-spectral similarity (cosine score ≥ 0.7) and the top 10 edges connecting one node were kept for each node. Molecular networks were visualized in Cytoscape (v 3.10.3)[46].

Features identified by mzmine were annotated with their molecular formulas and compound classification using CANOPUS[35] in the SIRIUS[38] *in silico* annotation tool (version 6.3.0 macOS arm64 build) following ClassyFire[47] taxonomy. De novo and bottom-up molecular formula assignments were performed for features with a m/z less than or greater than 400, respectively. Formulas for features with an m/z < 850 Da were predicted based on MS1 isotope pattern analysis and MS2 fragmentation tree analysis. All adducts were considered and adduct annotation was trusted.

2.4 DOC bioavailability assays

Following the incubations of the spring cohort, 1 L of incubation seawater was filtered through a pre-combusted 0.3 µm GF-75 and inoculated with 3.0 µm-filtered natural marine microbial community collected from the sea surface at Mohawk Reef in a ratio of 8:2. Assays were generated for each incubated blade (n = 24) and then partitioned into 12 pre-combusted 40mL glass vials. The vials were incubated in the dark near *in situ* temperatures (~13 - 14 ºC) and sampled as sacrificial parallel incubations at approximately 0, 7, 30 and 90 days. We define recalcitrant DOC as kelp-derived DOC that was not respired over this dark incubation period. Treatments were

incubated alongside seawater controls (n = 6) to account for the removal of ambient bioavailable DOC in either the initial ambient seawater or the microbial inoculum seawater. DOC samples were fixed with 60 µl 4N HCl and analyzed using a Shimadzu TOC-V or TOC-L according to Halewood et al.[48]. The bioavailability assay protocol had not yet been developed when our sampling of the summer cohort occurred so our bioavailability experiments reported here cover only the spring sampling period. During the summer period, we froze the exudates following the DOM exudation incubations, but after thawing, we observed precipitates in the seawater. As a result, we decided not to perform the bioavailability experiments due to the potential loss of DOM or changes to its composition that would bias the results. In the spring, we started the bioavailability assays immediately after finishing the exudation experiments.

2.5 Statistical analysis

To evaluate correlations between two variables, an ordinary least squares (OLS) linear regression was used if one variable was assumed not to have random variability (i.e. kelp age), but if both variables were assumed to have random error, then a Model II/Orthogonal Linear Regression was used. Principal coordinate analysis (PCoA) was computed using Bray Curtis measurements to visualize differences in the relative abundance of exudate molecular features between seasons and development stage. Permutational analysis of variance (PERMANOVA) was performed using the *adonis* from the R package vegan[49] to test if the relative abundance of molecular features was significantly different between season and developmental stage. Dispersion analysis was performed using the *betadisper* function in vegan to test if compared groups had

equal levels of within-group variance, respectively. Before the PCoA and PERMANOVA were performed, the relative abundances of molecular features across all samples were angular transformed and then standardized via z-scoring.

To compare the molecular composition of exudates at the compound class and subclass level, features were grouped as subnetworks based on the results of the feature-based molecular networking (FBMN) in GNPS2. For simplification, subnetworks were classified based on their subnetwork ID (component index output from GNPS2) and the compound class and subclass that were the dominant contributor to the subnetwork's relative abundance (i.e. 91; Phenols; Halophenols). Significant differences between two groups were measured using Student's t-test, Welch's t-test if variances were unequal, or the Wilcoxon Rank Sum test if observations were not normally distributed. All tests were considered significant at p-values < 0.05 and were adjusted using the Benjamini-Hochberg method where appropriate to account for false-discovery rates. All data visualization and statistical tests were performed in RStudio[50] or Cytoscape[46].

3. Results and Discussion

3.1 Environmental conditions and age structure giant kelp physiological state and productivity

In temperate coastal regions, kelp physiology and growth rates are driven by seasonal nitrate concentrations, light availability, and age-driven senescence[30,44]. In the summer where nitrate concentrations are typically below 1 μM, giant kelp accumulates biomass with high carbon-to-nitrogen content and low Chl:C, relative to spring time

upwelling conditions[51]. Further, giant kelp growth rates may become limited at nitrate concentrations less than 1 μM[30,44]. In addition to seasonally-driven variability in kelp physiology, giant kelp blades and fronds become senescent at around 50 days of age, regardless of ambient environmental conditions, and have an average lifespan of about 100 days[30,31,52].

Average daily temperatures and temperature-to-nitrate (T2N) estimated nitrate concentrations during our sampling period ranged from 11 – 20 ºC and 0.1 – 12 μM, respectively, and followed a typical annual trend at our study site[43]: warm summer conditions with low nitrate concentrations followed by springtime upwelling of cold, nitrate rich water (Figure 1A). The generalized additive model found a significant non-linear relationship between *in situ* temperature and measure nitrate concentrations at Mohawk Reef ($R^2 = 0.74$; $n = 210$; $p < 0.001$; Figure S3A), consistent with previous observations for the entire Southern California Bight region[41]. T2N estimates were significantly correlated with the nitrate concentrations measured monthly at Mohawk Reef ($R^2 = 0.74$, $y = 0.83x + 0.26$; Figure S3B). From our high-resolution T2N estimates, we observed that nitrate concentrations were consistently below 1 μM during the summer, whereas in the springtime, several upwelling events-maintained nitrate concentrations above this threshold, except for the very end of the spring cohort sampling period (Figure 1A).

We used kelp tissue C:N and Chl:C ratios as physiological proxies as they reflect seasonal nitrate availability and intrinsic biological processes such as senescence and are positively correlated with kelp growth rates, net primary production, and new frond initiation[44,53]. Kelp physiology responded significantly to seasonal environmental

conditions and developmental stage, consistent with previous studies[30,31,44]. Chl:C was significantly higher during the mature spring period compared to the summer ($p < 0.001$), but decreased non-linearly with age in both cohorts after 50 days of age (Figure 1B). We defined kelp as “mature” or “senescent” if the tissue was less than or older than 50 days of age, respectively. Tissue stoichiometric content (C:N) showed a similar pattern and was significantly higher in the summer mature period relative to the spring mature period ($p < 0.001$).

Maximum photosynthetic rates (P_{max}) declined linearly with age (Figure 1C) in both the spring (OLS; $R^2 = 0.44$, $p < 0.001$, $y = -1.3x + 177$, $n = 24$) and summer cohorts (OLS; $R^2 = 0.85$, $p < 0.001$, $y = -3.2 + 261$, $n = 30$). This rapid, non-linear decline in physiology followed the linear decline in maximum photosynthetic rates with age (Figure 1C), consistent with the patterns observed in senescing autotrophic organisms[54,55]. A decrease in maximum photosynthetic potential with age is predicted by optimization models of leaf-lifespan theory, which posits that photosynthetic appendages, i.e. blades, seek to maximize photosynthetic gains against maintenance and construction costs. Differences between the two seasonal cohorts, such as the initially higher P_{max}, steeper decline in P_{max}, and low tissue nitrogen in the summer relative to the spring (Figure 1C) are consistent with the predictions of leaf-life span theory[56]. These patterns may reflect giant kelp’s physiological adaptations to optimize photosynthetic gains across seasonal variability in light, nutrient concentrations and temperature. These results, along with a recent study that found kelps have a variable circadian rhythm with tissue age[57], suggest a dynamic physiology that should be considered to understand the role of kelps in coastal biogeochemistry.

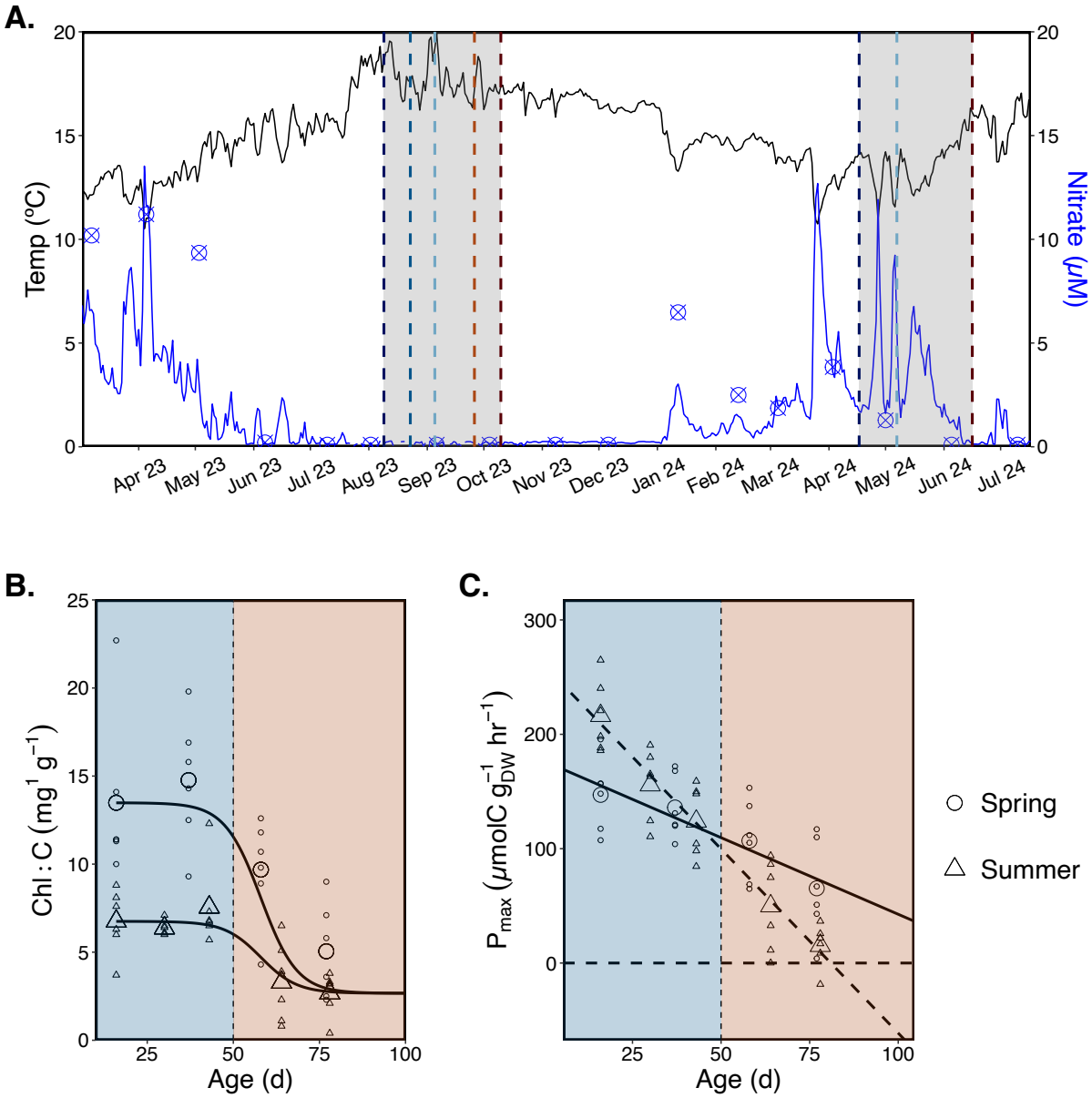

360

361 **Figure 1. Environmental conditions, kelp physiological state, and maximum photosynthetic**
362 **potential across the two seasonal cohorts and kelp age. (A)** Daily average temperature and
363 T2N-calculated nitrate concentrations across the study period. The grey shaded redions show the
364 specific sampling periods for the summer (Aug 23 – Oct 23) and spring (Apr 24 – Jun 24)
365 cohorts, respectively. Vertical dashed lines extending from the x-axis mark the sampling dates
366 for metabolomics measurments and the colors progress from dark blue to dark red in relation to
367 the age of the kelp tissue sampled. Blue circles with cross hairs (⊗) show the measured nitrate
368 concentrations from the SBC-LTER. Note that measured nitrate was below the limit of detection
369 (< 0.1 µM) throuhgout the summer period. **(B)** Age-related changes in the tissue chlorophyll
370 *a* to carbon (Chl:C) ratio in the spring and summer. The solid lines emphasize the non-
371 linear decline in Chl:C with age, beginning after 50 days. **(C)** Linear decrease in
372 maximum photosynthetic rate (P_{max}) with age in both spring and summer. The dashed

and solid regression lines show the significant negative linear relationship between P_{max} and age in the summer and spring, respectively. The dashed, horizontal line represents the transition between net respiration and net photosynthesis. Panel A is adapted from English et al., 2025, and panels **B** and **C** are adapted from English et al. 2025, respectively. In panels **B** and **C**, the larger circles and triangles represent the mean value for the replicate tissue samples (n = 6) at each age and seasonal cohort and the smaller shapes represent the individual measurements. Further, the blue and red shading on either side of 50 days represents the transition between mature and senescent kelp.

3.2 Exo-metabolite variability and stoichiometry

A primary producer's exudate composition reflects its response to environmental stimuli and developmental stage, including its acclimation to stress caused by nutrient limitation, temperature, microbial infection, or reactive oxygen species accumulation[27,28,58]. Using untargeted LC-MS/MS, we annotated a total of 26,191 (ESI+) and 17,184 (ESI-) molecular features, respectively, with unique mass and retention times. After filtering for features found in our process and analytical blanks and identifying features with a peak area >3 times than in the respective ambient seawater samples, 7,832 and 3,932 exudate features remained in the ESI+ and ESI- modes, respectively across our samples (n = 45). Exudate features were diverse and included peptides, fatty acyls, benzenoids, terpenoids, and aromatic organic halogens. We found that the relative abundance of the exudate features was significantly different between the developmental stages of giant kelp and season in both ESI+ (Figure 2A; PERMANOVA, $p < 0.001$, $R^2_{dev\_stage} = 0.13$, $R^2_{season} = 0.11$) and ESI- modes (Figure 2B; PERMANOVA, $p < 0.001$, $R^2_{dev\_stage} = 0.19$, $R^2_{season} = 0.13$). Gradients along the first principal coordinate axis explained 21.5 and 19.8% of the variability in the ESI+ and ESI-, respectively and were associated with kelp developmental stage (Figure 2). The second principal coordinate axis explained 16.1 and 12.9% of the variability in the ESI+

and ESI- mode, respectively and captured the seasonal variability in mature stage-kelp exudates (Figure 2). Exudate composition variability within each developmental stage was significantly higher in the mature stage compared to the senescent stage in both ESI+ and ESI- modes (R function *betadisper*; $p < 0.05$). This suggests seasonal drivers, such as temperature or nutrient availability influenced the composition of the mature stage-kelp exudates more than the senescent stage-kelp exudates.

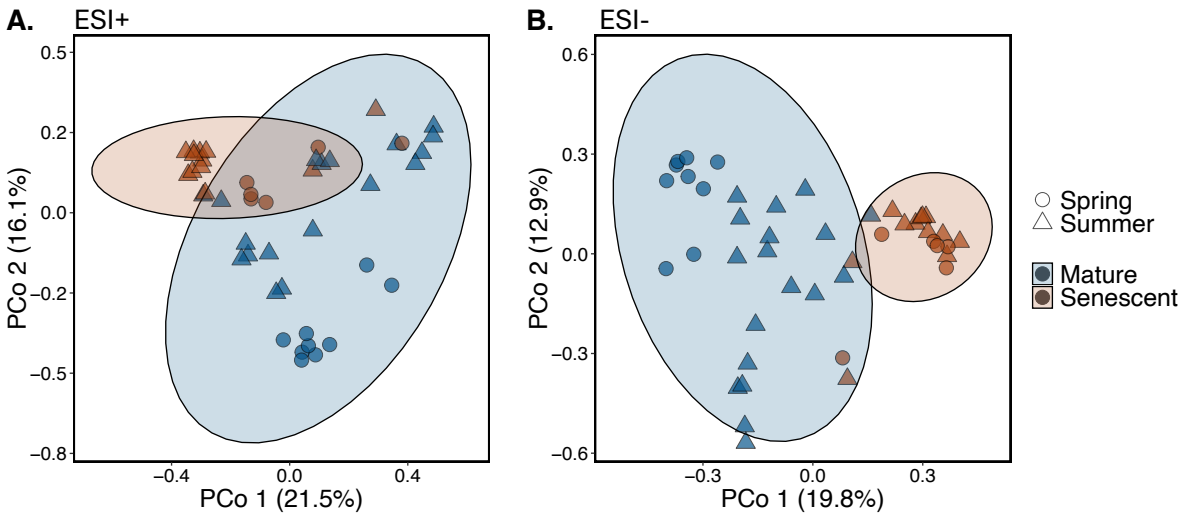

Figure 2. Giant kelp exudate composition is significantly different across developmental stages. Principal coordinate (PCo) analysis results (angular transformed and z-score normalized sample-centric relative abundances) for exudate features detected in the (**A**) positive (ESI+) and (**B**) negative (ESI-) electrospray ionization modes between developmental stage and season. Ellipses capture 95% of the data variability.

Major patterns across season and developmental stage included: 1) the exudate nitrogen content reflects seasonal and developmental stage gradients in nitrate availability, kelp age and physiology, and productivity and 2) the enhanced exudation of carbon and bromine-rich aromatic compounds and putative stress response compounds during senescence. Features containing carbon, hydrogen, oxygen and at least one

nitrogen (CHON) were the most abundant formulas in both and ESI- and ESI+ modes, and comprised between 29 and 90% of formulas across all samples. In both ionization modes, the proportion of CHON formulas significantly decreased between the mature and senescent developmental stages (Figure 3A and 3B; Wilcoxon Rank Sum, $p < 0.05$). In ESI+ and ESI-, the proportion of CHON formulas decreased from a mean of 75 and 65% to 66 and 43%, respectively after kelp became senescent. In both seasonal cohorts and ionization modes, the peak area weighted C:N of the exo-metabolites was significantly correlated to the C:N of the kelp tissue, and both increased as the kelp tissue aged (Figures 3C and 3D; $R^2 = 0.34 – 0.87$, $p < 0.001$). In ESI- mode, we observed a significantly lower weighted C:N of giant kelp exudates and a significantly lower proportion of N-containing formulas in the mature spring period compared to mature summer period, but this was not observed in the ESI+ mode (Figure 3A, 3B; Figure S4).

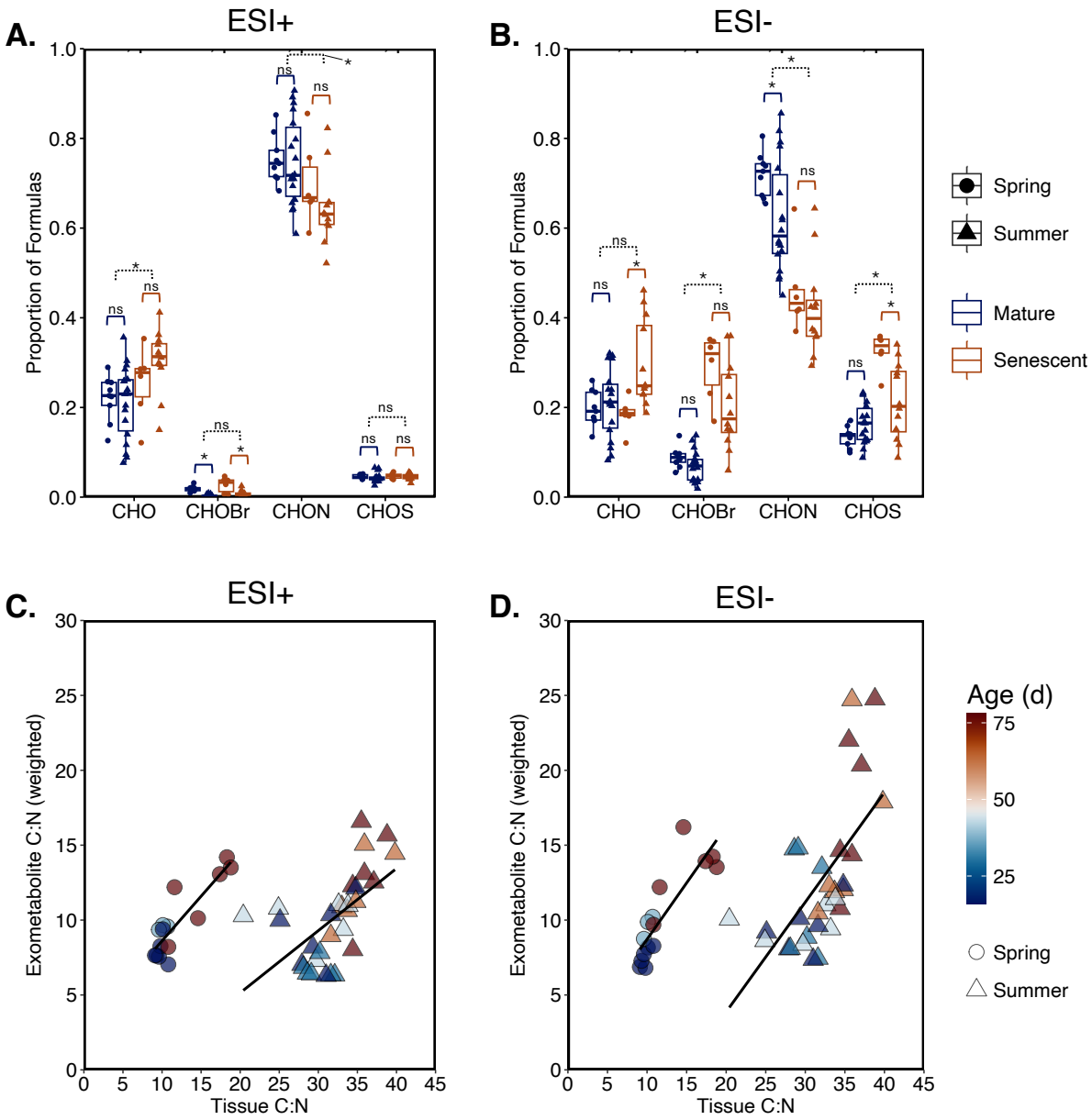

Figure 3: Exudate feature stoichiometry variation across developmental stage and season. Proportion of exudate feature formulas in the **(A)** ESI+ and **(B)** ESI- ionization modes that contain carbon, hydrogen, and oxygen (CHO), or at least one bromine (CHOBr), nitrogen (CHON), or sulfur (CHOS). Significant differences between the proportion of these formulas between developmental stage and season as determined by the Wilcoxon test are shown by asterisks with the following significance level indicators: ^{ns}not significant, *$p < 0.05$. Solid colored brackets show the results of the Wilcoxon test between seasons within each developmental stage and the black dashed brackets show the results of the Wilcoxon test between developmental stages. Significant correlations between the peak area weighted carbon to nitrogen (C:N) ratios of the exudates and the kelp tissue C:N ratios across seasons and age of the kelp tissue in the **(C)** positive and **(D)** negative ionizations modes.

Recent work with giant kelp demonstrates that older kelp tissue upregulates protein turnover compared to new tissue[57], suggesting that kelps regulate their nitrogen allocation in response to age, potentially in response to lower photosynthetic yields (Figure 1C)[59,60]. The exudation of nitrogen-rich compounds such as amino acids, dipeptides and peptides during the mature stage may function to establish and maintain host microbiomes[26,61]. Indeed, we found in our complementary study of these kelp samples, that the microbiome composition was significantly different between seasons and developmental stages[39]. The exudation of nitrogen-containing compounds may also, counterintuitively, serve to enhance the availability of inorganic nitrogen needed for kelp growth. For example, work with plant rhizospheres suggest that the exudation of nitrogen-rich metabolites primes the microbial hydrolysis of otherwise unavailable dissolved organic nitrogen (DON), resulting in a net increase in available nitrogen for growth[62]. Ammonification by microbial hydrolysis of DON may be an important source of recycled nitrogen that supports kelp growth, especially during the stratified summer periods[51]. In a study of bull kelp, the addition of ^{15}N labelled amino acids resulted in the accumulation of ^{15}N in the kelp tissue and $^{15}NH_4^+$ in seawater[63], presumably due to ammonification by the associated microbiome. This may explain why, in the summer, kelp released metabolites with a C:N two to three times lower than the tissue C:N, rather than invest that nitrogen into biomass (Figures 3C and 3D). However, it is unknown what fraction of nitrogen demand this would support relative to other processes such as the excretion of ammonia by benthic reef animals[51]. The increase in both tissue and exudate C:N in the summer and spring are consistent with the theorized

advantage of reallocating nitrogen-resources away from photosynthetic appendages with diminishing photosynthetic returns[52,64].

3.3 Associations between molecular families and developmental stage

Due to the diversity of DOM and the poor representation of compounds in spectral databases, we used feature-based molecular networking (FBMN) to uncover the structural composition of kelp-derived DOM across age-driven changes in kelp physiology. Through FBMN, features that network together have highly similar MS2 fragmentation spectra and therefore have a similar structural composition[37]. This networking increases the confidence in the feature formula and compound classification from the SIRIUS and CANOPUS outputs, and can be used to propagate the few spectral library matches across detected features. Results from FBMN of exo-metabolite features revealed clear compositional changes in response to kelp tissue age (Figure 4). In the ESI- mode, FBMN organized the 3,392 features into 436 subnetworks, or molecular families (Figure 4A). Many of these molecular families comprised a large fraction (>10%) of the total peak area of exudate features in each sample and were specific the either the mature or senescent developmental stage. The relative abundance of almost half (48%) of these subnetworks was significantly enriched during either developmental stage, suggesting the preferential exudation of specific compound classes by mature and senescent kelp (Figures 4B, 4C, and 4D; Wilcoxon Rank Sum test, FDR-adjusted $p < 0.05$). In the ESI- mode, these molecular families in the mature phase were enriched in included amino acids, peptides, and analogues and prenol lipids, while the senescent exudates were enriched in a number of aromatic

halocarbons, such as halophenols, aryl bromides, aryl chlorides, or halogenated benzoic acids (Figure 4D). Changes in the relative abundance of these major compound groups showed a clear response across the transition from the mature to senescent physiological state (Figures 5A and B). The increase in the relative abundance of halogenated phenols and aryl groups coincided with a significant increase (Wilcoxon test, $W = 15$, $p < 0.001$) in the peak area weighted bromine to carbon (Br:C) ratio during senescence (Figure 5C). Although the production of halogenated phenols was higher during senescence, we did observe the release of 3,5-Diiodo-L-tyrosine, 3-Iodo-L-tyrosine, and 3-Bromotyrosine preferentially during the mature kelp developmental stage (Figure 4C, Figure S5B). Halogenated tyrosines and their derivatives are widespread among marine organisms and exhibit diverse bioactivities, including antibacterial activity[65] and may play a role in kelp defense during the mature developmental stage.

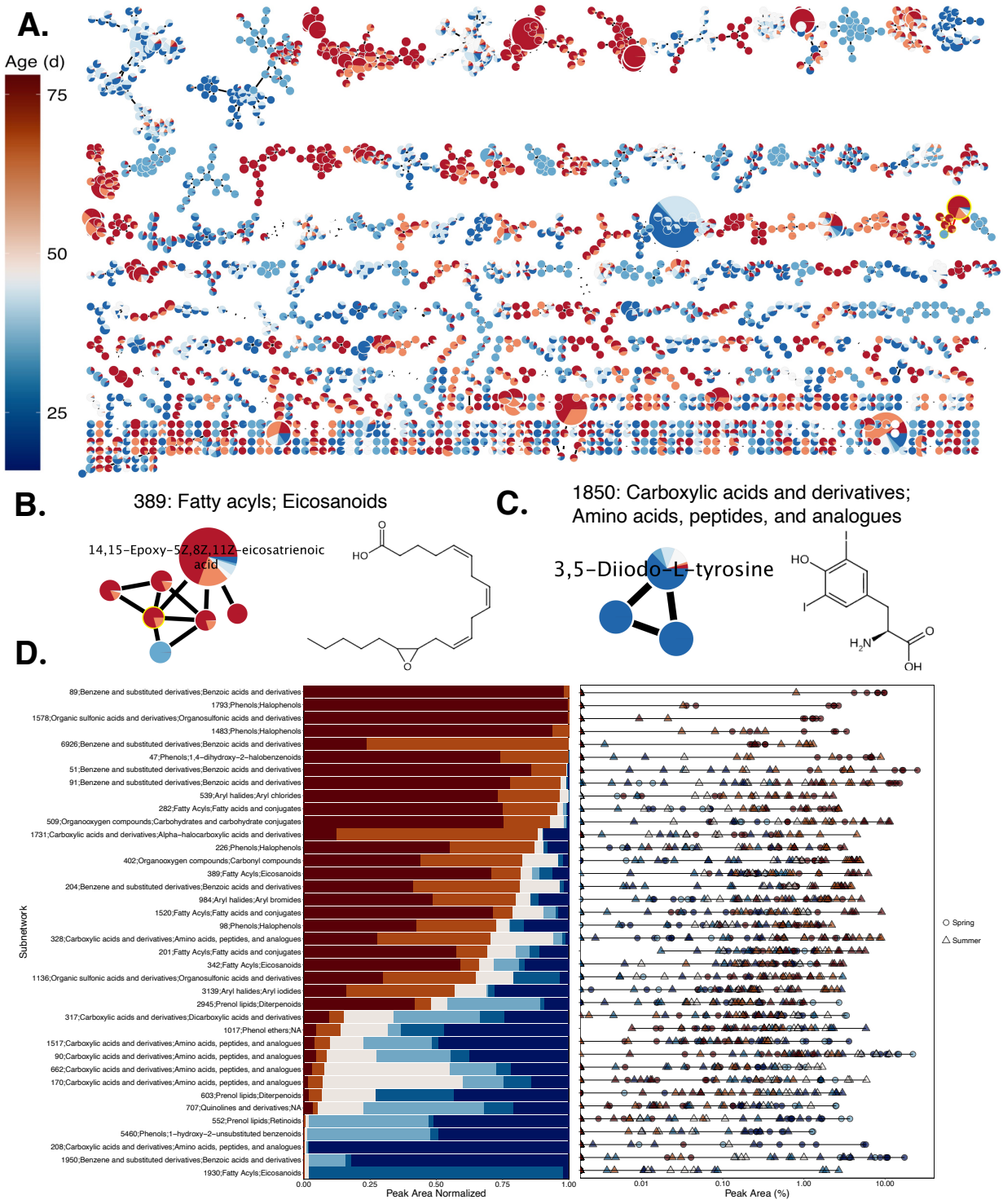

Figure 4. Molecular feature subnetworks detected in the negative electrospray ionization (ESI-) mode are significantly enriched across giant kelp developmental stage. (A) Network of all exudate features (nodes) linked by edges representing cosine similarity scores > 0.7 between nodes. Subnetworks are ordered by the number of nodes they contain and individual node sizes are scaled to their mean MS1 peak areas across all samples. Nodes are filled as pie

charts representing the relative MS1 peak area of that feature across different kelp ages. Representative FBMN subnetworks that contain features with matches to the NIST20 or GNPS2 spectral libraries are shown in **(B)** and **(C)** along with the structure of the library match. **(E)** Abundant subnetworks (mean peak area relative abundance > 1%) that are significantly different (Wilcoxon, FDR-adjusted $p < 0.05$) enriched between the mature and senescent kelp developmental stages. In the left panel, all subnetwork peak areas were normalized to 1 and the color shows the relative abundance of that subnetwork across the different ages (16, 30, 37, 43, 64, 77 & 78 days). The corresponding point and line plot to the right shows the range in subnetwork relative abundance across all samples in which the subnetwork was detected. Note the x-axis is log10 scaled.

During senescence, we observed an increase in the relative abundance of molecular families enriched in putative antimicrobial[66], antibiofilm[67], and immune function[68], including eicosanoids, halogenated phenols, fatty amides, furans, diterpenoids, and sulfonic acids (Figures 4D and S5D). In the ESI- mode, several subnetworks (Figure 4D; subnetworks 282, 389, 1520, 201, 342) enriched in eicosanoids and fatty acids had significantly higher relative abundances in senescent kelp exudates. Eicosanoids and fatty acids are putative immunolipids that regulate host-microbe symbiosis and host inflammation[33]. Studies of corals and macroalgae show that eicosanoids are produced in response to wounding[69] and regulate microbial-driven disease[70]. From FBMN and spectral matching to the NIST reference library, we found that giant kelp produces the eicosanoid 14,15-Epoxy-5Z,8Z,11Z-eicosatrienoic acid (14,15-EET) and structurally related compounds (Figures 4B and 4D; subnetwork 389) preferentially during senescence. EET's are known for their inhibition of cell adhesion and anti-inflammatory properties, particularly within the human vasculature system[71]. The production of 14,15-EET suggests kelp may also employ these compounds in respond to increased stress due to aging or microbial infection. Likewise, the increase in the production of sulfur-containing exudates during senescence suggests a defensive

response by kelp (Figure 3B). Previous work has shown that the production of sulfur containing metabolites by brown macroalgae can deter grazers, and may be produced in response to physical damage[72].

Putative defensive or stress-response compounds were also detected in the ESI+ mode data and included an increase in the relative abundance of molecular families enriched in aminoxides, diterpenoids, and lactams during senescence (Figure S5). In the ESI+ mode, 174 of the 977 subnetworks were significantly enriched in either developmental stage. Features classified as amino acids, peptides, or analogues were the most abundant and showed a similar trend in response to developmental stage as in the ESI- mode (Figure S6).

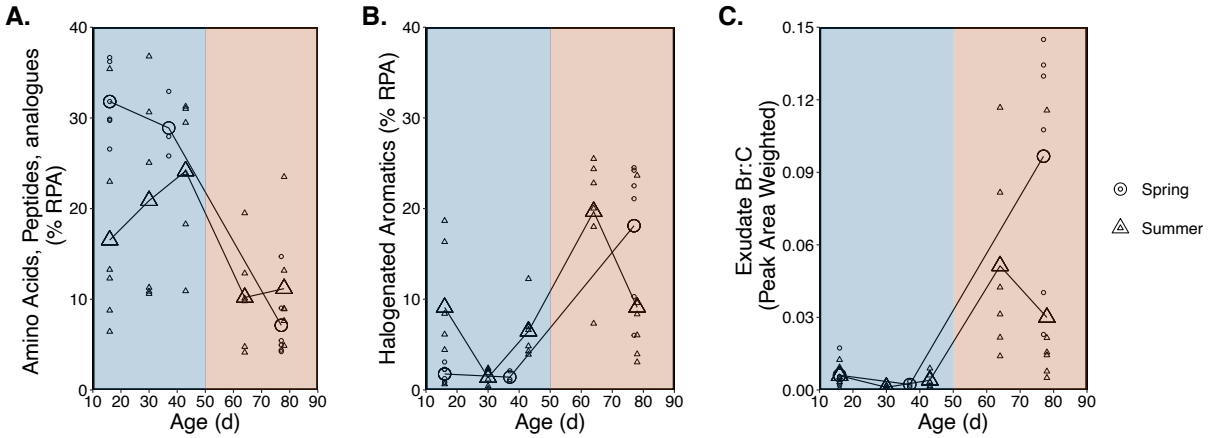

Figure 5. Major compound subclass relative abundance across kelp age and seasons in the ESI- analytical mode. The relative abudnance of compound subclasses across kelp age and season classified as **(A)** Amino acids, peptides, and analogues and **(B)** halogenated aromatics, including halophenols, aryl bromides, aryl iodides, aryl chlorides and halobenzoic acids. **(C)** The peak area weighted bromine to carbon (Br:C) ratio. Larger shapes indicate the mean value at each age and season and the smaller shapes represent the individual measurments.

568 *3.4 Kelps are a source of brominated dissolved organic matter*

569 Kelps are well known for their contribution to the marine halogen cycle and can
570 concentrate iodine and bromine to millimolar amounts in their tissues[73,74]. However, the
571 links between kelp halogen metabolism, dissolved organic matter biogeochemistry, and
572 carbon sequestration have yet to be explored. We observed an increase in the diversity
573 and abundance of brominated compounds as kelp became senescent (Figures 3B, 5B,
574 and S7). In the ESI- mode, features with at least one bromine (CHOBr) were 2 – 36% of
575 all formulas. On average, CHOBr were 8% of mature kelp exudate formulas, but
576 increased to 23% of formulas in the senescent kelp exudates (Figure 3B). In the ESI-
577 mode, we identified 594 exudate features that contained between 1 and 6 Br atoms.
578 Nearly half (48%) contained a single Br atom, 49% contained between 2 – 4 Br atoms
579 and about 2% contained 5 or 6 Br atoms. Mono- and poly-brominated phenols have
580 previously been observed in the exudates of the kelps *Eisenia bicyclis* and *Ecklonia*
581 *kurome*[75]. CHOBr formulas were rarer in the ESI+ mode results, making up on average
582 only 0.1 and 1.5% of formulas in the mature and senescent development stages,
583 respectively (Figure 3A). Compound classification of CHOBr features, based on the
584 Classyfire ontology, revealed that the majority were aromatics such as phenols and aryl
585 halides, consistent with their high oxygen to carbon (O:C) and low hydrogen to carbon
586 (H:C) ratios (Figure S7). These CHOBr molecular features had a similar range in O:C
587 and H:C stoichiometries as reported CHOBr features in the exudates of the brown algae
588 *Sargassum*[20], suggesting brown algae may be an important source of brominated
589 dissolved organic matter to the ocean.

While it is known that brown algae exude aromatic compounds, including phenols [9,75–77], the magnitude and controls on their production are poorly constrained[78]. The increase in the excretion of halogenated phenols, aryls and other benzenoids, (Figure 4D and 5B) is likely a response to stress experienced by senescing kelp. Little is known about the mechanisms behind giant kelp senescence, although the regular timing of its occurrence regardless of ambient environmental conditions[30,79] and its rapid onset following a linear decline in photosynthetic efficiency (Figure 1C) suggests some level of regulation similar to that of plants[60]. The decrease in the maximum photosynthetic potential observed with age can result in the accumulation of reactive oxygen species (ROS) at high irradiances[80] (Figure 1C). Under these conditions, ROS, such as hydrogen peroxide (H_2O_2), can accumulate and result in cell death[81,82]. Organisms have diverse mechanisms to reduce internal ROS concentrations. In kelps, this involves the use of vanadium-dependent haloperoxidases that catalyze the oxidation of halogens with hydrogen peroxide, resulting in the formation of halogenated organic compounds[83,84]. Bromoperoxidases from kelps and other algae catalyze the bromination of a wide range of compounds, including phenols and polyphenols such as phlorotannins[84–86], which would explain the increase in brominated phenols in senescent kelp exudates (Figures 4D and S7).

In addition to a byproduct of H_2O_2 detoxification, halogenated phenols and other haloperoxidase products are potent antimicrobial agents[87] as halogenation increases the bioactivity and antimicrobial effectiveness of phenols and other compounds[87–89]. In tandem with kelp entering its senescence phase, we observed, in a complementary study[39], a shift in the microbiome composition of these same kelp samples. This

involved an increase in the relative abundance of potential pathogens and the degradation of the alginate-rich cell wall, resulting in a pulse of oligoalginate degradation products. Therefore, an alternative mechanism for the exudation of halogenated aromatics during senescence may be the oxidative burst stress response[57,90,91]. In this pathway, microbial hydrolysis of the alginate-rich kelp cell-wall releases oligoalginates that trigger the production of H_2O_2 that is then scavenged by haloperoxidases. This mechanism is critical for kelp defense against microbial pathogens[90]. Consistent with the trigger of this pathway, we observed an increase in the abundance of molecular families enriched in carbohydrates in senescent giant kelp exudates (Subnetworks 509 and 1215 in Figures 4D and S5D, respectively) possibly due to alginate degradation products produced during senescence as we reported previously[31].

There has been extensive research on the production of short-lived volatile brominated compounds such as bromoform and dibromomethane by kelps due to their destruction of ozone[92]. The data presented here suggests kelps additionally release semi- or nonvolatile brominated compounds into the ocean that may contribute to the pool of recalcitrant DOC[93]. Previous work on the volatile halocarbons by kelps showed that the production was catalyzed by UV exposure[94], high irradiances[23], or increasing temperatures[95] consistent with the activity of bromoperoxidases during stress and H_2O_2 accumulation. Notably, outside of the senescent stage kelp, the highest abundance of halogenated aromatics in kelp exudates were observed during the summer cohort (Figure 5B). The relative abundance of these compounds was not constant across the mature summer kelp sampling period, but peaked around the highest seawater

636 temperatures of our sampling period (~ 19 ºC; Figure 1A, 5B). The production of
637 halogenated aromatics was low throughout the entire mature spring cohort sampling
638 period (Figure 5B) when temperatures were low and nitrate concentrations were high
639 (Figure 1A). Previous work demonstrated the production of methyl bromide and
640 bromoform also peaks in the summer[23].

641 While these mechanisms explain the enhanced production of halogenated
642 aromatics in senescent kelp DOM, it is unclear what will be the fate of this highly
643 brominated organic matter. Halogenated aromatics or their degradation byproducts are
644 often recalcitrant to microbial degradation[96]. For example, industrially-derived
645 brominated aromatics, such as the flame retardant Tetrabromobisphenol A or the anti-
646 fungal 2,4,6-tribromophenol, accumulate in the environment as a result of their chemical
647 inertness or incomplete microbial degredation[97,98]. Future work is needed to evaluate
648 the degradation of kelp-derived brominated aromatics.

649

650 *3.5 Recalcitrance of kelp-derived dissolved organic carbon (DOC)*

651 The proposed role of macroalgae in long-term carbon storage in the ocean is
652 based on the poorly constrained recalcitrance of released DOC[6,7]. This potential
653 recalcitrance has motivated proposals for macroalgal based carbon-dioxide removal in
654 the ocean; however, only a handful of studies have attempted to measure the fraction of
655 macroalgal-derived DOC that is recalcitrant[9,10,99–102], and fewer have considered the
656 role of kelp physiological condition in these estimates. In this study, we measured the
657 fraction of kelp-derived DOC from a spring kelp cohort that was recalcitrant across age-
658 dependent changes in kelp physiology and DOM composition. After the three-month

incubation period, we observed a recalcitrant fraction of kelp-derived DOC in every incubation (n = 24; Figure 6A). The percent of recalcitrant kelp-derived DOC ranged from 7-44% and averaged 19 ± 10% (Figure 6B). Bioavailable DOC was rapidly consumed within 7-30 days, with little change observed between 30 and 90 days. The fraction of DOC that was recalcitrant showed no significant correlation with the age of the kelp (Model II Regression; $R^2 = 0.03$, $p = 0.38$) or the concentration of kelp-derived DOC at the beginning of the incubation (Model II Regression; $R^2 = 0.11$, $p = 0.12$).

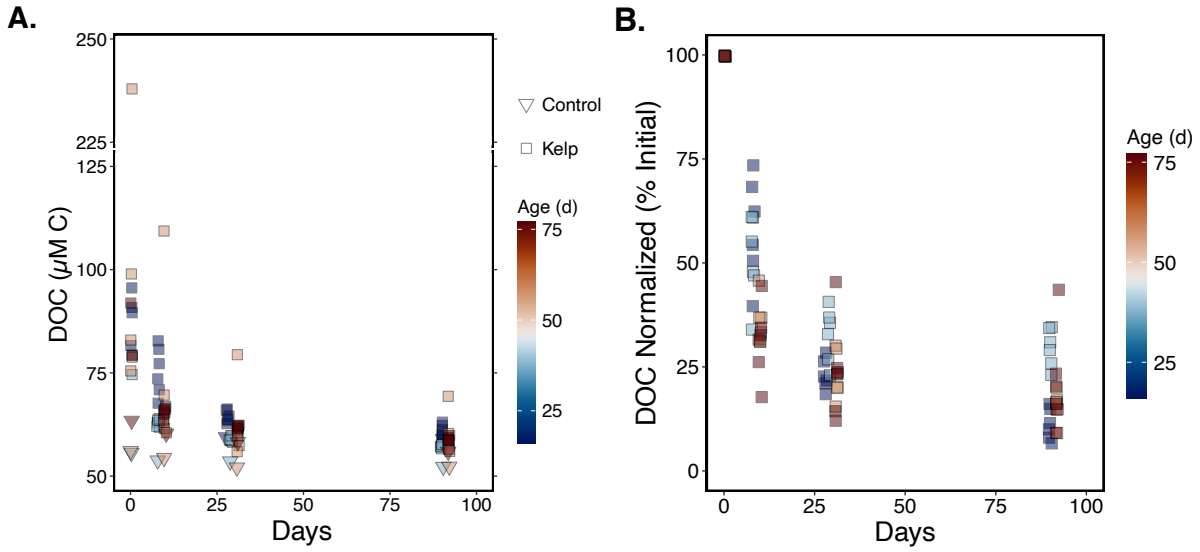

Figure 6. Bioavailability of kelp derived DOC in batch culture assays over three months. **(A)** Time-course of dissolved organic carbon (DOC) concentrations in the kelp-derived DOC (Kelp) and background DOC (Control) bioavailability assays. **(B)** Normalized kelp-derived DOC concentrations, corrected against the respective control incubations at each timepoint, over the three-month bioavailability assay. Points in both plots are slightly jittered at each timepoint for better visibility of the individual data points.

In our previous work we demonstrated that consideration of age-dependent senescence was critical to constrain the magnitude DOC production and potential for long-term carbon storage[31]. Likewise, we demonstrate that the composition of kelp-

678 derived DOC is dependent on the physiological state of kelp, driven by a combination of
679 seasonal abiotic forces and developmental stage. Molecular composition of DOC is a
680 main regulator of its recalcitrance and the data presented here clearly show that, while
681 much of the DOC released by kelp includes putatively labile compounds, such as
682 peptides and carbohydrates[12], kelps releases a diverse array of halogenated aromatic
683 compounds that may be more recalcitrant. A recent study observed that dissolved
684 organic bromines (DOBr) contribute to the marine refractory organic matter pool[93];
685 however, the molecular features identified in that study had lower oxygen to carbon
686 (O:C ~ 0.35) and higher hydrogen to carbon (H:C ~ 1.3) ratios than the DOBr observed
687 in our study (O:C ~ 0.2 - 1.0, H:C ~ 0.2 - 1.0; Figure S7A). This suggests deep-ocean
688 DOBr compounds are more aliphatic than aromatic compared to the freshly released
689 DOBr from kelps. In our previous study of *Sargassum*-derived DOM*,* we demonstrated
690 that phenolics are a component of biologically recalcitrant macroalgal-derived DOC,
691 although they were susceptible to photodegradation[101]. It is likely that sunlight can
692 degrade these halogenated aromatics into aliphatics[77,103] and produce compounds with
693 O:C and H:C ratios that resemble deep ocean DOBr. In addition, microbial metabolism
694 may produce degradation products resembling deep ocean DOBr by transforming the
695 aromatic ring into an aliphatic byproduct[104,105].

696 Despite large gradients in the stoichiometry and compound class relative
697 abundance of giant kelp exudates, we observed no significant variability in the
698 proportion of kelp-derived DOC that was recalcitrant to microbial remineralization in
699 response to kelp age (Figure 6). We note that our bioavailability experiments consider
700 only the spring cohort; however, both the spring and summer cohorts had similar shifts

in the stoichiometry and relative abundance of major compound classes in response to age (Figures 3, 5, and S6). The average proportion of giant kelp-derived DOC that was recalcitrant (19 ± 10%) is equal to the amount reported for cold-water kelps in a recent study (20 - 29%)[10], but lower than that reported for farmed *Saccharina japonica* (~ 37%)[102] and the assumed 33% first proposed by Krause-Jensen and Duarte (2016). The first study found a significant, but weak (R^2 = 0.10 – 0.16) correlation between the amount of recalcitrant DOC and the humic fluorescence signature of the exudates, suggesting compounds such as phenolics may drive the recalcitrance of the kelp-derived DOM.

The relative stability in the fraction of DOC that was recalcitrant in our study may be due to a number of reasons. First, although the transition to senescence resulted in an increase in halogenated aromatics and a decrease in nitrogen-rich compounds, there was also an increase in the amount of putatively labile compounds such as carbohydrates (Figure 4D). Second, it is likely that portions of each chemical class are labile and recalcitrant. For example, Quinlan et al.[106], observed that labile metabolites released by corals and macroalgae belong to diverse chemical classes such as benzenoids, organic acids and lipids. Lastly, our metabolomics approach using PPL column solid-phase extraction characterizes only a fraction of the total DOM pool (~25-65%)[19,107,108]. Therefore, differences in extraction and ionization efficiencies of molecules may prevent direct comparisons between the relative abundance of molecular families and bulk DOC remineralization assays. For example, although halogenated aromatics are likely enriched in senescent kelp exudates, their relative abundance may be inflated due to the generally higher extraction efficiencies of

aromatic compounds using PPL columns[108]. Additionally, a large fraction of kelp exudates are large polysaccharides that are not captured by our metabolomics approach. This includes large polymers (> 30 kDa) such as fucoidan, a biologically recalcitrant polysaccharide[109]. We previously observed that during senescence, the composition of kelp high molecular weight polysaccharide exudates shifts from the dominance of fucoidan to alginate that are more labile[31,110]. The production of more labile polysaccharides may compensate for the increased production of halogenated aromatics during senescence, resulting in a relatively fixed percentage of recalcitrant DOC produced by kelp (Figure 6B).

Regardless, compounds released during senescence likely account for an overall greater magnitude of DOC sequestration by kelps simply due to overall higher DOC production rates[31,32]. In our previous study, we estimated that senescence was responsible for ~ 75% of annual DOC production by giant kelp[31]. Therefore, the bromine-rich DOM produced by kelp during senescence may contribute significantly to marine carbon sequestration. However, more work is needed to demonstrate the degradation rates and products of these compounds by both biotic and abiotic sinks, including photodegradation which can remineralize biologically recalcitrant aromatics or transform them to more bioavailable products[77,101,111].

4. Environmental Implications

Coastal ocean ecosystems are dynamic biogeochemical regions and we are only just beginning to understand their global role[112]. Kelp forests are the largest coastal vegetated habitat globally[24,113], and it is critical that we identify processes controlling the

magnitude and composition of biogeochemical fluxes from these systems. This work reveals the diversity of kelp-derived DOM and provides new insights into the relationship between the physiological state and biogeochemistry of kelps that will guide future research into their long-term carbon storage potential. Our data supports recent work[10] suggesting that, on average, less than one third of kelp-derived DOM is recalcitrant to microbial remineralization. Additionally, the dynamic composition of kelp-derived DOM across environmental and physiological gradients reveals new avenues for research on the chemical ecology of kelp forests, especially as they respond to climate change, competition, grazing, or microbial disease[72,90,114–116]. Future work should explore the functional role of dissolved metabolites released by kelp, in particular the bromine-rich compounds, which may inform strategies for conservation, restoration, and large-scale aquaculture for marine carbon dioxide removal.

Acknowledgments

We thank the invaluable work of members of the Santa Barbara Coastal LTER whose data provided important background for our findings. We thank all Carlson lab members for the valuable discussion on the data. This project was funded by the Department of Energy's Advanced Research Project Agency-Energy through award DE-AR0001559 to DAS and CAC, and the National Science Foundation's Santa Barbara Coastal LTER through award number OCE-1831937 to DAS and CAC. D.P. was supported by the Simons Foundation International through a Simons Early Career Investigator in Aquatic Microbial Ecology and Evolution Award (SFI-LS-ECIAMEE-00013858).

Data and code availability

Data and code used for analysis, statistics and figure generations are available at https://github.com/chance-english/Giant_Kelp_DOC. Data for Mohawk Reef temperature and nitrate concentrations are available through the Santa Barbara Coastal LTER data portal (sbclter.msi.ucsb.edu/data/catalog/). All raw and processed LC-MS/MS data as well as processed MS/MS files are available through the Mass Spectrometry Interactive Virtual Environment (MassIVE) repository (massive.ucsd.edu) with accession number MSV000095805. Task ID's for the feature based molecular networking in the GNPS2 dashboard in ESI+ and ESI- mode are 5f967b24848243828cfd4d8302725a7a and 945866a72f1a4f9895b23df5eba32e42.

Competing Interests

The authors declare no competing interests.

References

(1) Duarte, C. M.; Gattuso, J.-P.; Hancke, K.; Gundersen, H.; Filbee-Dexter, K.; Pedersen, M. F.; Middelburg, J. J.; Burrows, M. T.; Krumhansl, K. A.; Wernberg, T.; Moore, P.; Pessarrodona, A.; Ørberg, S. B.; Pinto, I. S.; Assis, J.; Queirós, A. M.; Smale, D. A.; Bekkby, T.; Serrão, E. A.; Krause-Jensen, D. Global Estimates of the Extent and Production of Macroalgal Forests. *Glob. Ecol. Biogeogr.* **2022**, *31* (7), 1422–1439. https://doi.org/10.1111/geb.13515.

(2) Smith, S. V. Marine Macrophytes as a Global Carbon Sink. *Sci. New Ser.* **1981**, *211* (4484), 838–840.

(3) National Academies of Sciences, Engineering, and Medicine. A Research Strategy for Ocean-Based Carbon Dioxide Removal and Sequestration. **2022**. https://doi.org/https://doi.org/10.17226/26278.

(4) Ricart, A. M.; Krause-Jensen, D.; Hancke, K.; Price, N. N.; Masqué, P.; Duarte, C. M. Sinking Seaweed in the Deep Ocean for Carbon Neutrality Is Ahead of Science and beyond the Ethics. *Environ. Res. Lett.* **2022**, *17* (8), 081003. https://doi.org/10.1088/1748-9326/ac82ff.

(5) Sten, M.; Yamamoto, K.; DeVries, T.; Krause, S. J. E.; Siegel, D. A. On the Efficiency and Durability of Purposefully Sinking Seaweed Biomass as a Marine Carbon Dioxide Removal Strategy. *Earths Future* **2026**, *14* (5), e2025EF007628. https://doi.org/10.1029/2025EF007628.

(6) Krause-Jensen, D.; Duarte, C. M. Substantial Role of Macroalgae in Marine Carbon Sequestration. *Nat. Geosci.* **2016**, *9* (10), 737–742. https://doi.org/10.1038/ngeo2790.

(7) Krumhansl, K. A.; Wong, M. C.; Picard, M. M. M.; Fraser, M.; Gabriel, C.-E.; Wu, Y.; Azetsu-Scott, K. Blue Carbon Sequestration Dominated by Dissolved Organic Carbon Pathways for Kelp Forests and Eelgrass Meadows in Nova Scotia, Canada. *Commun. Earth Environ.* **2026**, *7* (1), 98. https://doi.org/10.1038/s43247-025-03122-2.

(8) Li, H.; Zhang, Z.; Xiong, T.; Tang, K.; He, C.; Shi, Q.; Jiao, N.; Zhang, Y. Carbon Sequestration in the Form of Recalcitrant Dissolved Organic Carbon in a Seaweed (Kelp) Farming Environment. *Environ. Sci. Technol.* **2022**, *56* (12), 9112–9122. https://doi.org/10.1021/acs.est.2c01535.

(9) Wada, S.; Aoki, M.; Mikami, A.; Komatsu, T.; Tsuchiya, Y.; Sato, T.; Shinagawa, H.; Hama, T. Bioavailability of Macroalgal Dissolved Organic Matter in Seawater. *Mar. Ecol. Prog. Ser.* **2008**, *370*, 33–44. https://doi.org/10.3354/meps07645.

(10) Watanabe, K.; Hori, M.; Kubo, A.; Moki, H.; Kuwae, T. Macroalgal and Seagrass Species Generate Variable Amounts of Recalcitrant Dissolved Organic Carbon in Coastal Japan. *Commun. Earth Environ.* **2026**, *7* (1), 456. https://doi.org/10.1038/s43247-026-03600-1.

(11) Shen, Y.; Benner, R. Molecular Properties Are a Primary Control on the Microbial Utilization of Dissolved Organic Matter in the Ocean. *Limnol. Oceanogr.* **2020**, *65* (5), 1061–1071. https://doi.org/10.1002/lno.11369.

(12) Dittmar, T.; Lennartz, S. T. Reasons behind the Long-Term Stability of Dissolved Organic Matter. In *Biogeochemistry of Marine Dissolved Organic Matter*; Elsevier, 2024; pp 613–655. https://doi.org/10.1016/B978-0-443-13858-4.00006-X.
(13) Kloareg, B.; Quatrano, R. S. Structure of the Cell Walls of Marine Algae and Ecophysiological Functions of the Matrix Polysaccharides. *Oceanogr. Mar. Biol. Annu. Rev.* **1988**, *26*, 259–315.
(14) Saha, M.; Goecke, F.; Bhadury, P. Minireview: Algal Natural Compounds and Extracts as Antifoulants. *J. Appl. Phycol.* **2018**, *30* (3), 1859–1874. https://doi.org/10.1007/s10811-017-1322-0.
(15) Peteiro, C. Alginate Production from Marine Macroalgae, with Emphasis on Kelp Farming. In *Alginates and Their Biomedical Applications*; Rehm, B. H. A., Moradali, M. F., Eds.; Springer: Singapore, 2018; pp 27–66. https://doi.org/10.1007/978-981-10-6910-9_2.
(16) Topcu, G.; Aydogmus, Z.; Imre, S.; Gören, A. C.; Pezzuto, J. M.; Clement, J. A.; Kingston, D. G. I. Brominated Sesquiterpenes from the Red Alga *Laurencia o Btusa*. *J. Nat. Prod.* **2003**, *66* (11), 1505–1508. https://doi.org/10.1021/np030176p.
(17) Greff, S.; Zubia, M.; Genta-Jouve, G.; Massi, L.; Perez, T.; Thomas, O. P. Mahorones, Highly Brominated Cyclopentenones from the Red Alga Asparagopsis Taxiformis. *J. Nat. Prod.* **2014**, *77* (5), 1150–1155. https://doi.org/10.1021/np401094h.
(18) Ford, L.; Stratakos, A. Ch.; Theodoridou, K.; Dick, J. T. A.; Sheldrake, G. N.; Linton, M.; Corcionivoschi, N.; Walsh, P. J. Polyphenols from Brown Seaweeds as a Potential Antimicrobial Agent in Animal Feeds. *ACS Omega* **2020**, *5* (16), 9093–9103. https://doi.org/10.1021/acsomega.9b03687.
(19) Wegley Kelly, L.; Nelson, C. E.; Petras, D.; Koester, I.; Quinlan, Z. A.; Arts, M. G. I.; Nothias, L.-F.; Comstock, J.; White, B. M.; Hopmans, E. C.; Van Duyl, F. C.; Carlson, C. A.; Aluwihare, L. I.; Dorrestein, P. C.; Haas, A. F. Distinguishing the Molecular Diversity, Nutrient Content, and Energetic Potential of Exometabolomes Produced by Macroalgae and Reef-Building Corals. *Proc. Natl. Acad. Sci.* **2022**, *119* (5). https://doi.org/10.1073/pnas.2110283119.
(20) Powers, L. C.; Hertkorn, N.; McDonald, N.; Schmitt-Kopplin, P.; Del Vecchio, R.; Blough, N. V.; Gonsior, M. Sargassum Sp. Act as a Large Regional Source of Marine Dissolved Organic Carbon and Polyphenols. *Glob. Biogeochem. Cycles* **2019**, *33* (11), 1423–1439. https://doi.org/10.1029/2019GB006225.
(21) Wada, S.; Aoki, M. N.; Tsuchiya, Y.; Sato, T.; Shinagawa, H.; Hama, T. Quantitative and Qualitative Analyses of Dissolved Organic Matter Released from *Ecklonia Cava* Kjellman, in Oura Bay, Shimoda, Izu Peninsula, Japan. *J. Exp. Mar. Biol. Ecol.* **2007**, *349* (2), 344–358. https://doi.org/10.1016/j.jembe.2007.05.024.
(22) Abdullah, M. I.; Fredriksen, S. Production, Respiration and Exudation of Dissolved Organic Matter by the Kelp Laminaria Hyperborea along the West Coast of Norway. *J. Mar. Biol. Assoc. U. K.* **2004**, *84* (5), 887–894. https://doi.org/10.1017/S002531540401015Xh.
(23) Goodwin, K. D.; North, W. J.; Lidstrom, M. E. Production of Bromoform and Dibromomethane by Giant Kelp: Factors Affecting Release and Comparison to

Anthropogenic Bromine Sources. *Limnol. Oceanogr.* **1997**, *42* (8), 1725–1734. https://doi.org/10.4319/lo.1997.42.8.1725.
(24) Pessarrodona, A.; Assis, J.; Filbee-Dexter, K.; Burrows, M. T.; Gattuso, J.-P.; Duarte, C. M.; Krause-Jensen, D.; Moore, P. J.; Smale, D. A.; Wernberg, T. Global Seaweed Productivity. *Sci. Adv.* **2022**, *8* (37), eabn2465. https://doi.org/10.1126/sciadv.abn2465.
(25) Duarte, C. M.; Bruhn, A.; Krause-Jensen, D. A Seaweed Aquaculture Imperative to Meet Global Sustainability Targets. *Nat. Sustain.* **2022**, *5* (3), 185–193. https://doi.org/10.1038/s41893-021-00773-9.
(26) Zhalnina, K.; Louie, K. B.; Hao, Z.; Mansoori, N.; da Rocha, U. N.; Shi, S.; Cho, H.; Karaoz, U.; Loqué, D.; Bowen, B. P.; Firestone, M. K.; Northen, T. R.; Brodie, E. L. Dynamic Root Exudate Chemistry and Microbial Substrate Preferences Drive Patterns in Rhizosphere Microbial Community Assembly. *Nat. Microbiol.* **2018**, *3* (4), 470–480. https://doi.org/10.1038/s41564-018-0129-3.
(27) Baker, N. R.; Zhalnina, K.; Yuan, M.; Herman, D.; Ceja-Navarro, J. A.; Sasse, J.; Jordan, J. S.; Bowen, B. P.; Wu, L.; Fossum, C.; Chew, A.; Fu, Y.; Saha, M.; Zhou, J.; Pett-Ridge, J.; Northen, T. R.; Firestone, M. K. Nutrient and Moisture Limitations Reveal Keystone Metabolites Linking Rhizosphere Metabolomes and Microbiomes. *Proc. Natl. Acad. Sci.* **2024**, *121* (32). https://doi.org/10.1073/pnas.2303439121.
(28) Bais, H. P.; Weir, T. L.; Perry, L. G.; Gilroy, S.; Vivanco, J. M. THE ROLE OF ROOT EXUDATES IN RHIZOSPHERE INTERACTIONS WITH PLANTS AND OTHER ORGANISMS. *Annu. Rev. Plant Biol.* **2006**, *57* (1), 233–266. https://doi.org/10.1146/annurev.arplant.57.032905.105159.
(29) Bell, T. W.; Cavanaugh, K. C.; Reed, D. C.; Siegel, D. A. Geographical Variability in the Controls of Giant Kelp Biomass Dynamics. *J. Biogeogr.* **2015**, *42* (10), 2010–2021. https://doi.org/10.1111/jbi.12550.
(30) Bell, T. W.; Siegel, D. A. Nutrient Availability and Senescence Spatially Structure the Dynamics of a Foundation Species. *Proc. Natl. Acad. Sci.* **2022**, *119* (1), e2105135118. https://doi.org/10.1073/pnas.2105135118.
(31) English, C. J.; Bell, T. W.; Opalk, K.; Siegel, D. A.; Carlson, C. A. Senescence-Driven Solubilization of Biomass Is the Main Source of Kelp-Derived Dissolved Organic Carbon to the Coastal Ocean. *Commun. Biol.* **2025**, *8* (1), 1172. https://doi.org/10.1038/s42003-025-08477-y.
(32) Carlson, A. K.; Yoshimura, T.; Kudo, I. Kelp Dissolved Organic Carbon Release Is Seasonal and Annually Enhanced during Senescence. *J. Phycol.* **2024**, *60* (4), 980–1000. https://doi.org/10.1111/jpy.13483.
(33) Mannochio-Russo, H.; Swift, S. O. I.; Nakayama, K. K.; Wall, C. B.; Gentry, E. C.; Panitchpakdi, M.; Caraballo-Rodriguez, A. M.; Aron, A. T.; Petras, D.; Dorrestein, K.; Dorrestein, T. K.; Williams, T. M.; Nalley, E. M.; Altman-Kurosaki, N. T.; Martinelli, M.; Kuwabara, J. Y.; Darcy, J. L.; Bolzani, V. S.; Wegley Kelly, L.; Mora, C.; Yew, J. Y.; Amend, A. S.; McFall-Ngai, M.; Hynson, N. A.; Dorrestein, P. C.; Nelson, C. E. Microbiomes and Metabolomes of Dominant Coral Reef Primary Producers Illustrate a Potential Role for Immunolipids in Marine Symbioses. *Commun. Biol.* **2023**, *6* (1), 896. https://doi.org/10.1038/s42003-023-05230-1.

(34) Petras, D.; Koester, I.; Da Silva, R.; Stephens, B. M.; Haas, A. F.; Nelson, C. E.; Kelly, L. W.; Aluwihare, L. I.; Dorrestein, P. C. High-Resolution Liquid Chromatography Tandem Mass Spectrometry Enables Large Scale Molecular Characterization of Dissolved Organic Matter. *Front. Mar. Sci.* **2017**, *4*, 405. https://doi.org/10.3389/fmars.2017.00405.

(35) Dührkop, K.; Nothias, L.-F.; Fleischauer, M.; Reher, R.; Ludwig, M.; Hoffmann, M. A.; Petras, D.; Gerwick, W. H.; Rousu, J.; Dorrestein, P. C.; Böcker, S. Systematic Classification of Unknown Metabolites Using High-Resolution Fragmentation Mass Spectra. *Nat. Biotechnol.* **2021**, *39* (4), 462–471. https://doi.org/10.1038/s41587-020-0740-8.

(36) Schmid, R.; Heuckeroth, S.; Korf, A.; Smirnov, A.; Myers, O.; Dyrlund, T. S.; Bushuiev, R.; Murray, K. J.; Hoffmann, N.; Lu, M.; Sarvepalli, A.; Zhang, Z.; Fleischauer, M.; Dührkop, K.; Wesner, M.; Hoogstra, S. J.; Rudt, E.; Mokshyna, O.; Brungs, C.; Ponomarov, K.; Mutabdžija, L.; Damiani, T.; Pudney, C. J.; Earll, M.; Helmer, P. O.; Fallon, T. R.; Schulze, T.; Rivas-Ubach, A.; Bilbao, A.; Richter, H.; Nothias, L.-F.; Wang, M.; Orešič, M.; Weng, J.-K.; Böcker, S.; Jeibmann, A.; Hayen, H.; Karst, U.; Dorrestein, P. C.; Petras, D.; Du, X.; Pluskal, T. Integrative Analysis of Multimodal Mass Spectrometry Data in MZmine 3. *Nat. Biotechnol.* **2023**, *41* (4), 447–449. https://doi.org/10.1038/s41587-023-01690-2.

(37) Nothias, L.-F.; Petras, D.; Schmid, R.; Dührkop, K.; Rainer, J.; Sarvepalli, A.; Protsyuk, I.; Ernst, M.; Tsugawa, H.; Fleischauer, M.; Aicheler, F.; Aksenov, A. A.; Alka, O.; Allard, P.-M.; Barsch, A.; Cachet, X.; Caraballo-Rodriguez, A. M.; Da Silva, R. R.; Dang, T.; Garg, N.; Gauglitz, J. M.; Gurevich, A.; Isaac, G.; Jarmusch, A. K.; Kameník, Z.; Kang, K. B.; Kessler, N.; Koester, I.; Korf, A.; Le Gouellec, A.; Ludwig, M.; Martin H., C.; McCall, L.-I.; McSayles, J.; Meyer, S. W.; Mohimani, H.; Morsy, M.; Moyne, O.; Neumann, S.; Neuweger, H.; Nguyen, N. H.; Nothias-Esposito, M.; Paolini, J.; Phelan, V. V.; Pluskal, T.; Quinn, R. A.; Rogers, S.; Shrestha, B.; Tripathi, A.; van der Hooft, J. J. J.; Vargas, F.; Weldon, K. C.; Witting, M.; Yang, H.; Zhang, Z.; Zubeil, F.; Kohlbacher, O.; Böcker, S.; Alexandrov, T.; Bandeira, N.; Wang, M.; Dorrestein, P. C. Feature-Based Molecular Networking in the GNPS Analysis Environment. *Nat. Methods* **2020**, *17* (9), 905–908. https://doi.org/10.1038/s41592-020-0933-6.

(38) Dührkop, K.; Fleischauer, M.; Ludwig, M.; Aksenov, A. A.; Melnik, A. V.; Meusel, M.; Dorrestein, P. C.; Rousu, J.; Böcker, S. SIRIUS 4: A Rapid Tool for Turning Tandem Mass Spectra into Metabolite Structure Information. *Nat. Methods* **2019**, *16* (4), 299–302. https://doi.org/10.1038/s41592-019-0344-8.

(39) English, C. J.; Manoj, M.; Henderson, L. C.; Opalk, K.; Carlson, C. A. Seasonal and Developmental Stage Changes in Mucilage Carbohydrate Content Shape the Kelp Microbiome. *ISME Commun.* **2025**, *5* (1), ycaf197. https://doi.org/10.1093/ismeco/ycaf197.

(40) Santa Barbara Coastal LTER; Reed, D. C. SBC LTER: Reef: Bottom Temperature: Continuous Water Temperature, Ongoing since 2000, 2025. https://doi.org/https://doi.org/10.6073/pasta/c3ec3193ba97e7670b532cfbbe1632f9.

(41) Snyder, J. N.; Bell, T. W.; Siegel, D. A.; Nidzieko, N. J.; Cavanaugh, K. C. Sea Surface Temperature Imagery Elucidates Spatiotemporal Nutrient Patterns for Offshore Kelp

Aquaculture Siting in the Southern California Bight. *Front. Mar. Sci.* **2020**, *7*. https://doi.org/10.3389/fmars.2020.00022.
(42) Wood, S. Mgcv: Mixed GAM Computation Vehicle with Automatic Smoothness Estimation, 2025. https://cran.r-project.org/web/packages/mgcv/index.html (accessed 2026-06-09).
(43) Washburn, L.; Brzezinski, M. A.; Carlson, C. A.; Siegel, D. A. SBC LTER: Ocean: Ocean Currents and Biogeochemistry: Nearshore Water Profiles (Monthly CTD and Chemistry), Ongoing since 2000, 2026. https://doi.org/10.6073/PASTA/FBBC4C52781D2E6CE336ECC16DF1CB7C.
(44) Bell, T. W.; Reed, D. C.; Nelson, N. B.; Siegel, D. A. Regional Patterns of Physiological Condition Determine Giant Kelp Net Primary Production Dynamics. *Limnol. Oceanogr.* **2018**, *63* (1), 472–483. https://doi.org/10.1002/lno.10753.
(45) Seely, G. R.; Duncan, M. J.; Vidaver, W. E. Preparative and Analytical Extraction of Pigments from Brown Algae with Dimethyl Sulfoxide. *Mar. Biol.* **1972**, *12* (2), 184–188. https://doi.org/10.1007/BF00350754.
(46) Shannon, P.; Markiel, A.; Ozier, O.; Baliga, N. S.; Wang, J. T.; Ramage, D.; Amin, N.; Schwikowski, B.; Ideker, T. Cytoscape: A Software Environment for Integrated Models of Biomolecular Interaction Networks. *Genome Res.* **2003**, *13* (11), 2498–2504. https://doi.org/10.1101/gr.1239303.
(47) Djoumbou Feunang, Y.; Eisner, R.; Knox, C.; Chepelev, L.; Hastings, J.; Owen, G.; Fahy, E.; Steinbeck, C.; Subramanian, S.; Bolton, E.; Greiner, R.; Wishart, D. S. ClassyFire: Automated Chemical Classification with a Comprehensive, Computable Taxonomy. *J. Cheminformatics* **2016**, *8*, 61. https://doi.org/10.1186/s13321-016-0174-y.
(48) Halewood, E.; Opalk, K.; Custals, L.; Carey, M.; Hansell, D. A.; Carlson, C. A. Determination of Dissolved Organic Carbon and Total Dissolved Nitrogen in Seawater Using High Temperature Combustion Analysis. *Front. Mar. Sci.* **2022**, *9*. https://doi.org/10.3389/fmars.2022.1061646.
(49) Oksanen, J.; Simpson, G. L.; Blanchet, F. G.; Kindt, R.; Legendre, P.; Minchin, P. R.; O'Hara, R. B.; Solymos, P.; Stevens, M. H. H.; Szoecs, E.; Wagner, H.; Barbour, M.; Bedward, M.; Bolker, B.; Borcard, D.; Borman, T.; Carvalho, G.; Chirico, M.; Caceres, M. D.; Durand, S.; Evangelista, H. B. A.; FitzJohn, R.; Friendly, M.; Furneaux, B.; Hannigan, G.; Hill, M. O.; Lahti, L.; Martino, C.; McGlinn, D.; Ouellette, M.-H.; Cunha, E. R.; Smith, T.; Stier, A.; Braak, C. J. F. T.; Weedon, J. Vegan: Community Ecology Package, 2026. https://cran.r-project.org/web/packages/vegan/index.html (accessed 2026-05-19).
(50) Posit team. RStudio: Integrated Development Environment for R., 2025. http://www.posit.co/. (accessed 2026-05-19).
(51) Brzezinksi, M.; Reed, D.; Harrer, S.; Rassweiler, A.; Melack, J.; Goodridge, B.; Dugan, J. Multiple Sources and Forms of Nitrogen Sustain Year-Round Kelp Growth on the Inner Continental Shelf of the Santa Barbara Channel. *Oceanography* **2013**, *26* (3), 114–123. https://doi.org/10.5670/oceanog.2013.53.

(52) Rodriguez, G. E.; Reed, D. C.; Holbrook, S. J. Blade Life Span, Structural Investment, and Nutrient Allocation in Giant Kelp. *Oecologia* **2016**, *182* (2), 397–404. https://doi.org/10.1007/s00442-016-3674-6.
(53) Shivji, M. S. Interactive Effects of Light and Nitrogen on Growth and Chemical Composition of Juvenile Macrocystis Pyrifera (L.) C. Ag. (Phaeophyta) Sporophytes. *J. Exp. Mar. Biol. Ecol.* **1985**, *89* (1), 81–96. https://doi.org/10.1016/0022-0981(85)90083-8.
(54) Kitajima, K.; Mulkey, S. S.; Wright, S. J. Decline of Photosynthetic Capacity with Leaf Age in Relation to Leaf Longevities for Five Tropical Canopy Tree Species. *Am. J. Bot.* **1997**, *84* (5), 702–708. https://doi.org/10.2307/2445906.
(55) Chabot, B. F.; Hicks, D. J. The Ecology of Leaf Life Spans. *Annu. Rev. Ecol. Syst.* **1982**, *13* (1), 229–259. https://doi.org/10.1146/annurev.es.13.110182.001305.
(56) Kikuzawa, K. A Cost-Benefit Analysis of Leaf Habit and Leaf Longevity of Trees and Their Geographical Pattern. *Am. Nat.* **1991**, *138* (5), 1250–1263. https://doi.org/10.1086/285281.
(57) Chandra, M. I.; Nuzhdin, S. V.; Gracey, A. Y. Differential Transcriptomic and Circadian Regulation across Giant Kelp Blades Based on Relative Tissue Age. *J. Phycol.* **2026**, *62* (2), 329–346. https://doi.org/10.1111/jpy.70137.
(58) Olofsson, M.; Uchimiya, M.; Ferrer-González, F. X.; Schreier, J. E.; Powers, M. A.; Smith, C. B.; Edison, A. S.; Moran, M. A. Dynamic Reworking of Marine Diatom Endometabolomes in Response to Temperature and a Model Bacterium. *mSystems* **2025**, *11* (1), e01036-25. https://doi.org/10.1128/msystems.01036-25.
(59) Schippers, J. H. M.; Schmidt, R.; Wagstaff, C.; Jing, H.-C. Living to Die and Dying to Live: The Survival Strategy behind Leaf Senescence1. *Plant Physiol.* **2015**, *169* (2), 914–930. https://doi.org/10.1104/pp.15.00498.
(60) Thomas, H. Senescence, Ageing and Death of the Whole Plant. *New Phytol.* **2013**, *197* (3), 696–711. https://doi.org/10.1111/nph.12047.
(61) Van de Velde, W.; Zehirov, G.; Szatmari, A.; Debreczeny, M.; Ishihara, H.; Kevei, Z.; Farkas, A.; Mikulass, K.; Nagy, A.; Tiricz, H.; Satiat-Jeunemaître, B.; Alunni, B.; Bourge, M.; Kucho, K.; Abe, M.; Kereszt, A.; Maroti, G.; Uchiumi, T.; Kondorosi, E.; Mergaert, P. Plant Peptides Govern Terminal Differentiation of Bacteria in Symbiosis. *Science* **2010**, *327* (5969), 1122–1126. https://doi.org/10.1126/science.1184057.
(62) Drake, J. E.; Darby, B. A.; Giasson, M.-A.; Kramer, M. A.; Phillips, R. P.; Finzi, A. C. Stoichiometry Constrains Microbial Response to Root Exudation- Insights from a Model and a Field Experiment in a Temperate Forest. *Biogeosciences* **2013**, *10* (2), 821–838. https://doi.org/10.5194/bg-10-821-2013.
(63) Hochroth, A.; Pfister, C. A. Ammonification by Kelp Associated Microbes Increases Ammonium Availability. *PloS One* **2024**, *19* (3), e0296622. https://doi.org/10.1371/journal.pone.0296622.
(64) Nelson, C. J.; Millar, A. H. Protein Turnover in Plant Biology. *Nat. Plants* **2015**, *1* (3), 15017. https://doi.org/10.1038/nplants.2015.17.
(65) Ferreira Montenegro, P.; Pham, G. N.; Abdoul-Latif, F. M.; Taffin-de-Givenchy, E.; Mehiri, M. Marine Bromotyrosine Derivatives in Spotlight: Bringing Discoveries and

Biological Significance. *Mar. Drugs* **2024**, *22* (3), 132. https://doi.org/10.3390/md22030132.
(66) Sakami, T. Effects of Algal Excreted Substances on the Respiration Activities of Epiphytic Bacteria on the Brown Alga, *Eisenia Bicyclis* Kjellman. *Fish. Sci.* **1996**, *62* (3), 394–396. https://doi.org/10.2331/fishsci.62.394.
(67) Maximilien, R.; Nys, R. de; Holmström, C.; Gram, L.; Givskov, M.; Crass, K.; Kjelleberg, S.; Steinberg, P. D. Chemical Mediation of Bacterial Surface Colonisation by Secondary Metabolites from the Red Alga Delisea Pulchra. *Aquat. Microb. Ecol.* **1998**, *15*, 233–246. https://doi.org/10.3354/ame015233.
(68) Dennis, E. A.; Norris, P. C. Eicosanoid Storm in Infection and Inflammation. *Nat. Rev. Immunol.* **2015**, *15* (8), 511–523. https://doi.org/10.1038/nri3859.
(69) Lõhelaid, H.; Teder, T.; Tõldsepp, K.; Ekins, M.; Samel, N. Up-Regulated Expression of AOS-LOXa and Increased Eicosanoid Synthesis in Response to Coral Wounding. *PLOS ONE* **2014**, *9* (2), e89215. https://doi.org/10.1371/journal.pone.0089215.
(70) Bouarab, K.; Adas, F.; Gaquerel, E.; Kloareg, B.; Salaün, J.-P.; Potin, P. The Innate Immunity of a Marine Red Alga Involves Oxylipins from Both the Eicosanoid and Octadecanoid Pathways. *Plant Physiol.* **2004**, *135* (3), 1838–1848. https://doi.org/10.1104/pp.103.037622.
(71) Node, K.; Huo, Y.; Ruan, X.; Yang, B.; Spiecker, M.; Ley, K.; Zeldin, D. C.; Liao, J. K. Anti-Inflammatory Properties of Cytochrome P450 Epoxygenase-Derived Eicosanoids. *Science* **1999**, *285* (5431), 1276–1279. https://doi.org/10.1126/science.285.5431.1276.
(72) Schnitzler, I.; Boland, W.; Hay, M. E. Organic Sulfur Compounds from Dictyopteris Spp. Deter Feeding by an Herbivorous Amphipod (Ampithoe Longimana) but Not by an Herbivorous Sea Urchin (Arbacia Punctulata). *J. Chem. Ecol.* **1998**, *24* (10), 1715–1732. https://doi.org/10.1023/A:1020876830580.
(73) Saenko, G. N.; Kravtsova, Y. Y.; Ivanenko, V. V.; Sheludko, S. I. Concentration of Lodine and Bromine by Plants in the Seas of Japan and Okhotsk. *Mar. Biol.* **1978**, *47* (3), 243–250. https://doi.org/10.1007/BF00541002.
(74) Küpper, F. C.; Carpenter, L. J.; McFiggans, G. B.; Palmer, C. J.; Waite, T. J.; Boneberg, E.-M.; Woitsch, S.; Weiller, M.; Abela, R.; Grolimund, D.; Potin, P.; Butler, A.; Luther, G. W.; Kroneck, P. M. H.; Meyer-Klaucke, W.; Feiters, M. C. Iodide Accumulation Provides Kelp with an Inorganic Antioxidant Impacting Atmospheric Chemistry. *Proc. Natl. Acad. Sci.* **2008**, *105* (19), 6954–6958. https://doi.org/10.1073/pnas.0709959105.
(75) Shibata, T.; Hama, Y.; Miyasaki, T.; Ito, M.; Nakamura, T. Extracellular Secretion of Phenolic Substances from Living Brown Algae. *J. Appl. Phycol.* **2006**, *18* (6), 787–794. https://doi.org/10.1007/s10811-006-9094-y.
(76) Carlson, D. J. Surface Microlayer Phenolic Enrichments Indicate Sea Surface Slicks. *Nature* **1982**, *296* (5856), 426–429. https://doi.org/10.1038/296426a0.
(77) Powers, L. C.; Del Vecchio, R.; Blough, N. V.; McDonald, N.; Schmitt-Kopplin, P.; Gonsior, M. Optical Properties and Photochemical Transformation of the Dissolved Organic Matter Released by Sargassum. *Front. Mar. Sci.* **2020**, *7*, 588287. https://doi.org/10.3389/fmars.2020.588287.

(78) Jennings, J. G.; Steinberg, P. D. In Situ Exudation of Phlorotannins by the Sublittoral Kelp Ecklonia Radiata. *Mar. Biol.* **1994**, *121* (2), 349–354. https://doi.org/10.1007/BF00346744.
(79) Rodriguez, G. E.; Rassweiler, A.; Reed, D. C.; Holbrook, S. J. The Importance of Progressive Senescence in the Biomass Dynamics of Giant Kelp (Macrocystis Pyrifera). *Ecology* **2013**, *94* (8), 1848–1858. https://doi.org/10.1890/12-1340.1.
(80) Van Breusegem, F.; Dat, J. F. Reactive Oxygen Species in Plant Cell Death. *Plant Physiol.* **2006**, *141* (2), 384–390. https://doi.org/10.1104/pp.106.078295.
(81) Chandra, J.; Samali, A.; Orrenius, S. Triggering and Modulation of Apoptosis by Oxidative Stress. *Free Radic. Biol. Med.* **2000**, *29* (3), 323–333. https://doi.org/10.1016/S0891-5849(00)00302-6.
(82) Bidle, K. D.; Falkowski, P. G. Cell Death in Planktonic, Photosynthetic Microorganisms. *Nat. Rev. Microbiol.* **2004**, *2* (8), 643–655. https://doi.org/10.1038/nrmicro956.
(83) Soedjak, H. S.; Butler, A. Characterization of Vanadium Bromoperoxidase from Macrocystis and Fucus: Reactivity of Vanadium Bromoperoxidase toward Acyl and Alkyl Peroxides and Bromination of Amines. *Biochemistry* **1990**, *29* (34), 7974–7981. https://doi.org/10.1021/bi00486a028.
(84) Butler, A.; Soedjak, H. S.; Polne-Fuller, M.; Gibor, A.; Boyen, C.; Kloareg, B. Studies of Vandadium-Bromoperoxidase Using Surface and Cortical Protoplasts of Macrocystis Pyriefera (Phaeophyta). *J. Phycol.* **1990**, *26* (3), 589–592. https://doi.org/10.1111/j.0022-3646.1990.00589.x.
(85) Wischang, D.; Hartung, J. Bromination of Phenols in Bromoperoxidase-Catalyzed Oxidations. *Tetrahedron* **2012**, *68* (46), 9456–9463. https://doi.org/10.1016/j.tet.2012.08.081.
(86) Yamada, H.; Itoh, N.; Murakami, S.; Izumi, Y. New Bromoperoxidase from Coralline Algae That Brominates Phenol Compounds. *Agric. Biol. Chem.* **1985**, *49* (10), 2961–2967. https://doi.org/10.1080/00021369.1985.10867194.
(87) Gribble, G. W. Biological Activity of Recently Discovered Halogenated Marine Natural Products. *Mar. Drugs* **2015**, *13* (7), 4044–4136. https://doi.org/10.3390/md13074044.
(88) Fraise, A. P. Choosing Disinfectants. *J. Hosp. Infect.* **1999**, *43* (4), 255–264. https://doi.org/10.1016/S0195-6701(99)90421-8.
(89) Han, J.; Li, W.; Zhang, X. An Effective and Rapidly Degradable Disinfectant from Disinfection Byproducts. *Nat. Commun.* **2024**, *15* (1), 4888. https://doi.org/10.1038/s41467-024-48752-w.
(90) Küpper, F. C.; Müller, D. G.; Peters, A. F.; Kloareg, B.; Potin, P. Oligoalginate Recognition and Oxidative Burst Play a Key Role in Natural and Induced Resistance of Sporophytes of Laminariales. *J. Chem. Ecol.* **2002**, *28* (10), 2057–2081. https://doi.org/10.1023/A:1020706129624.
(91) Küpper, F. C.; Kloareg, B.; Guern, J.; Potin, P. Oligoguluronates Elicit an Oxidative Burst in the Brown Algal Kelp Laminaria Digitata. *Plant Physiol.* **2001**, *125* (1), 278–291. https://doi.org/10.1104/pp.125.1.278.
(92) Yung, Y. L.; Pinto, J. P.; Watson, R. T.; Sander, S. P. Atmospheric Bromine and Ozone Perturbations in the Lower Stratosphere. **1980**.

(93) Powers, L. C.; Schijf, J.; Schmitt-Kopplin, P.; Gonsior, M. Halogenated Organic Compounds: A Massive Halogen Reservoir and an Intriguing Component of the Marine Dissolved Organic Matter Pool. *Geophys. Res. Lett.* **2026**, *53* (1), e2025GL119062. https://doi.org/10.1029/2025GL119062.
(94) Laturnus, F.; Svensson, T.; Wiencke, C. Release of Reactive Organic Halogens by the Brown Macroalga Saccharina Latissima after Exposure to Ultraviolet Radiation. *Polar Res.* **2010**, *29* (3), 379–384. https://doi.org/10.3402/polar.v29i3.6075.
(95) Mehrtens, G.; Laturnus, F. Halogenating Activity in an Arctic Population of Brown Macroalga Laminaria Saccharina (L.) Lamour. *Polar Res.* **1997**, *16* (1), 19–26. https://doi.org/10.3402/polar.v16i1.6622.
(96) Commandeur, L. C. M.; Parsons, J. R. Degradation of Halogenated Aromatic Compounds. *Biodegradation* **1990**, *1* (2), 207–220. https://doi.org/10.1007/BF00058837.
(97) Ronen, Z.; Abeliovich, A. Anaerobic-Aerobic Process for Microbial Degradation of Tetrabromobisphenol A. *Appl. Environ. Microbiol.* **2000**, *66* (6), 2372–2377. https://doi.org/10.1128/AEM.66.6.2372-2377.2000.
(98) Zhang, Q.; Liu, Y.; Lin, Y.; Kong, W.; Zhao, X.; Ruan, T.; Liu, J.; Schnoor, J. L.; Jiang, G. Multiple Metabolic Pathways of 2,4,6-Tribromophenol in Rice Plants. *Environ. Sci. Technol.* **2019**, *53* (13), 7473–7482. https://doi.org/10.1021/acs.est.9b01514.
(99) Watanabe, K.; Yoshida, G.; Hori, M.; Umezawa, Y.; Moki, H.; Kuwae, T. Macroalgal Metabolism and Lateral Carbon Flows Can Create Significant Carbon Sinks. *Biogeosciences* **2020**, *17* (9), 2425–2440. https://doi.org/10.5194/bg-17-2425-2020.
(100) Li, H.; Zhang, Z.; Xiong, T.; Tang, K.; He, C.; Shi, Q.; Jiao, N.; Zhang, Y. Carbon Sequestration in the Form of Recalcitrant Dissolved Organic Carbon in a Seaweed (Kelp) Farming Environment. *Environ. Sci. Technol.* **2022**, *56* (12), 9112–9122. https://doi.org/10.1021/acs.est.2c01535.
(101) English, C. J.; Parsons, R.; Yongblah, K.; Opalk, K.; Carlson, C. A. Photooxidation Removes Biologically Recalcitrant Dissolved Organic Carbon Released by the Macroalga Sargassum Natans. *Limnol. Oceanogr. Lett.* **2025**, *10* (3), 349–359. https://doi.org/10.1002/lol2.70011.
(102) Gao, Y.; Zhang, Y.; Du, M.; Lin, F.; Jiang, W.; Li, W.; Li, F.; Lv, X.; Fang, J.; Jiang, Z. Dissolved Organic Carbon from Cultured Kelp Saccharina Japonica: Production, Bioavailability, and Bacterial Degradation Rates. *Aquac. Environ. Interact.* **2021**, *13*, 101–110. https://doi.org/10.3354/aei00393.
(103) Ward, C. P.; Cory, R. M. Complete and Partial Photo-Oxidation of Dissolved Organic Matter Draining Permafrost Soils. *Environ. Sci. Technol.* **2016**, *50* (7), 3545–3553. https://doi.org/10.1021/acs.est.5b05354.
(104) Häggblom, M. M. Microbial Breakdown of Halogenated Aromatic Pesticides and Related Compounds. *FEMS Microbiol. Rev.* **1992**, *9* (1), 29–71. https://doi.org/10.1111/j.1574-6968.1992.tb05823.x.
(105) Ghosal, D.; You, I.-S.; Chatterjee, D. K.; Chakrabarthy, A. M. Microbial Degradation of Halogenated Compounds. *Science* **1985**, *228* (4696), 135–142.
(106) Quinlan, Z. A.; Nelson, C. E.; Koester, I.; Petras, D.; Nothias, L.; Comstock, J.; White, B. M.; Aluwihare, L. I.; Bailey, B. A.; Carlson, C. A.; Dorrestein, P. C.; Haas, A. F.;

Wegley Kelly, L. Microbial Community Metabolism of Coral Reef Exometabolomes Broadens the Chemodiversity of Labile Dissolved Organic Matter. *Environ. Microbiol.* **2025**, *27* (3), e70064. https://doi.org/10.1111/1462-2920.70064.

(107) Dittmar, T.; Koch, B.; Hertkorn, N.; Kattner, G. A Simple and Efficient Method for the Solid-Phase Extraction of Dissolved Organic Matter (SPE-DOM) from Seawater. *Limnol. Oceanogr. Methods* **2008**, *6* (6), 230–235. https://doi.org/10.4319/lom.2008.6.230.

(108) Johnson, W. M.; Kido Soule, M. C.; Kujawinski, E. B. Extraction Efficiency and Quantification of Dissolved Metabolites in Targeted Marine Metabolomics. *Limnol. Oceanogr. Methods* **2017**, *15* (4), 417–428. https://doi.org/10.1002/lom3.10181.

(109) Sichert, A.; Corzett, C. H.; Schechter, M. S.; Unfried, F.; Markert, S.; Becher, D.; Fernandez-Guerra, A.; Liebeke, M.; Schweder, T.; Polz, M. F.; Hehemann, J.-H. Verrucomicrobia Use Hundreds of Enzymes to Digest the Algal Polysaccharide Fucoidan. *Nat. Microbiol.* **2020**, *5* (8), 1026–1039. https://doi.org/10.1038/s41564-020-0720-2.

(110) Zhang, Y.-S.; Zhang, Y.-Q.; Zhao, X.-M.; Liu, X.-L.; Qin, Q.-L.; Liu, N.-H.; Xu, F.; Chen, X.-L.; Zhang, Y.-Z.; Li, P.-Y. Metagenomic Insights into the Dynamic Degradation of Brown Algal Polysaccharides by Kelp-Associated Microbiota. *Appl. Environ. Microbiol.* **2024**, *90* (2). https://doi.org/10.1128/aem.02025-23.

(111) Kong, H. L.; Sayler, G. S. Degradation and Total Mineralization of Monohalogenated Biphenyls in Natural Sediment and Mixed Bacterial Culture. *Appl. Environ. Microbiol.* **1983**, *46* (3), 666–672. https://doi.org/10.1128/aem.46.3.666-672.1983.

(112) Ward, N. D.; Megonigal, J. P.; Bond-Lamberty, B.; Bailey, V. L.; Butman, D.; Canuel, E. A.; Diefenderfer, H.; Ganju, N. K.; Goñi, M. A.; Graham, E. B.; Hopkinson, C. S.; Khangaonkar, T.; Langley, J. A.; McDowell, N. G.; Myers-Pigg, A. N.; Neumann, R. B.; Osburn, C. L.; Price, R. M.; Rowland, J.; Sengupta, A.; Simard, M.; Thornton, P. E.; Tzortziou, M.; Vargas, R.; Weisenhorn, P. B.; Windham-Myers, L. Representing the Function and Sensitivity of Coastal Interfaces in Earth System Models. *Nat. Commun.* **2020**, *11* (1), 2458. https://doi.org/10.1038/s41467-020-16236-2.

(113) Duarte, C. M.; Losada, I. J.; Hendriks, I. E.; Mazarrasa, I.; Marbà, N. The Role of Coastal Plant Communities for Climate Change Mitigation and Adaptation. *Nat. Clim. Change* **2013**, *3* (11), 961–968. https://doi.org/10.1038/nclimate1970.

(114) Arafeh-Dalmau, N.; Schoeman, D. S.; Montaño-Moctezuma, G.; Micheli, F.; Rogers-Bennett, L.; Olguin-Jacobson, C.; Possingham, H. P. Marine Heat Waves Threaten Kelp Forests. *Science* **2020**, *367* (6478), 635–635. https://doi.org/10.1126/science.aba5244.

(115) Farrell, S. P.; Petras, D.; Stincone, P.; Yiu, D. S.; Burns, J. A.; Pakkir Shah, A. K.; Hartmann, A. C.; Brady, D. C.; Rasher, D. B. Turf Algae Redefine the Chemical Landscape of Temperate Reefs, Limiting Kelp Forest Recovery. *Science* **2025**, *388* (6749), 876–880. https://doi.org/10.1126/science.adt6788.

(116) Steinberg, P. D. Algal Chemical Defense against Herbivores: Allocation of Phenolic Compounds in the Kelp Alaria Marginata. *Science* **1984**, *223* (4634), 405–407.

Supplemental Figures

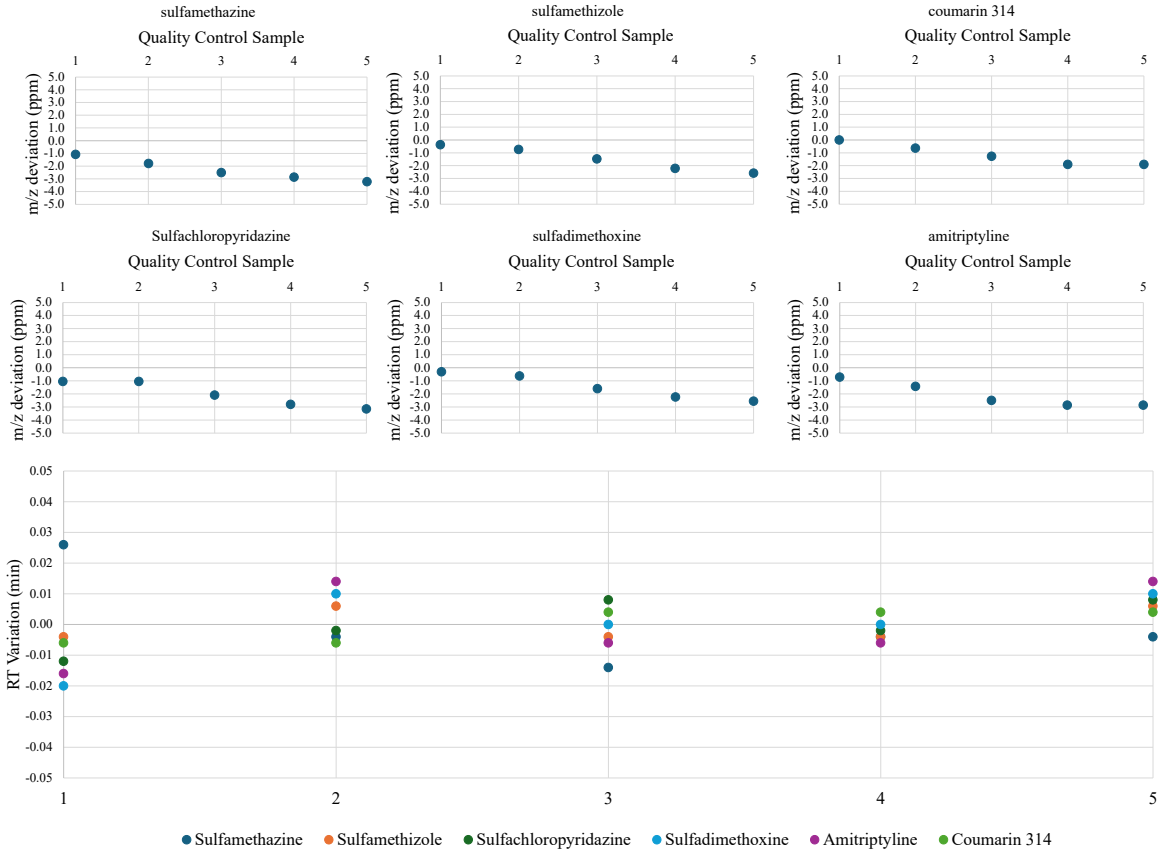

Figure S1. Quality control for ESI+ UHPLC-MS/MS. (A) m/z and **(B)** retention time deviations for samples run in the ESI+ mode. The six standard compounds were run every 10 samples. The x-axis on all plot are the QC sample number run every 10 samples.

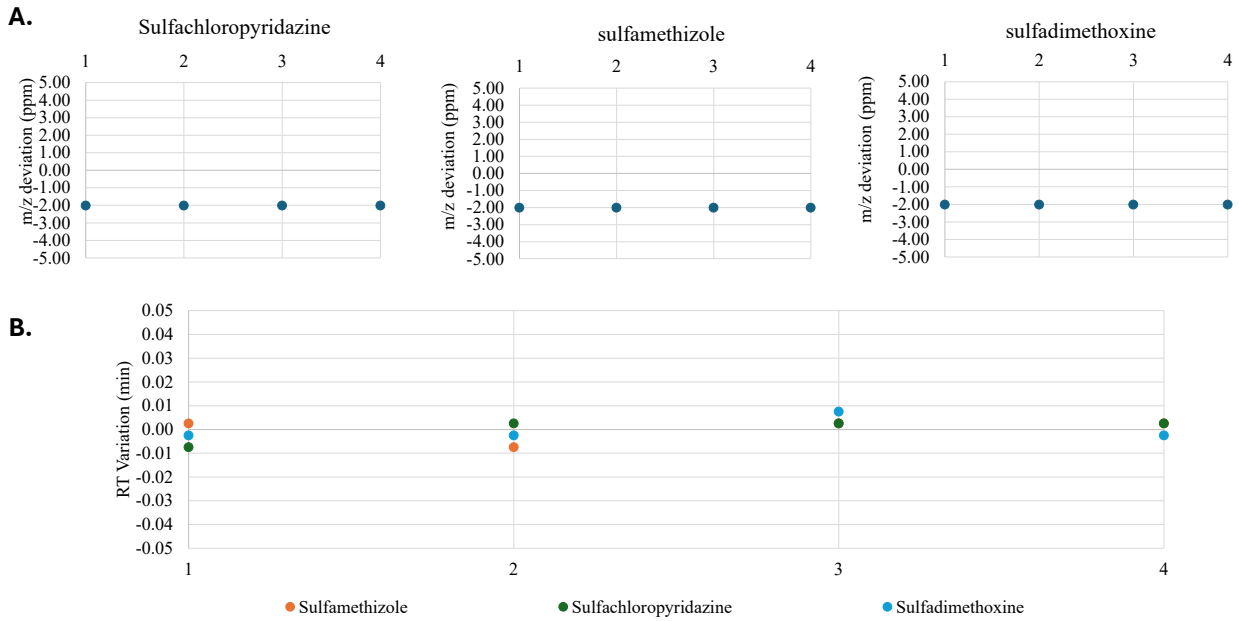

Figure S2. Quality control for ESI- UHPLC-MS/MS. (A) m/z and **(B)** retention time deviations for samples run in the ESI- mode. The standard compounds were run every 10 samples. The x-axis on all plot shows the QC sample number run every 10 samples. The internal standards sulfamethazine, amitriptyline, coumarin 314 were not observed in the negative mode annotations from mzmine.

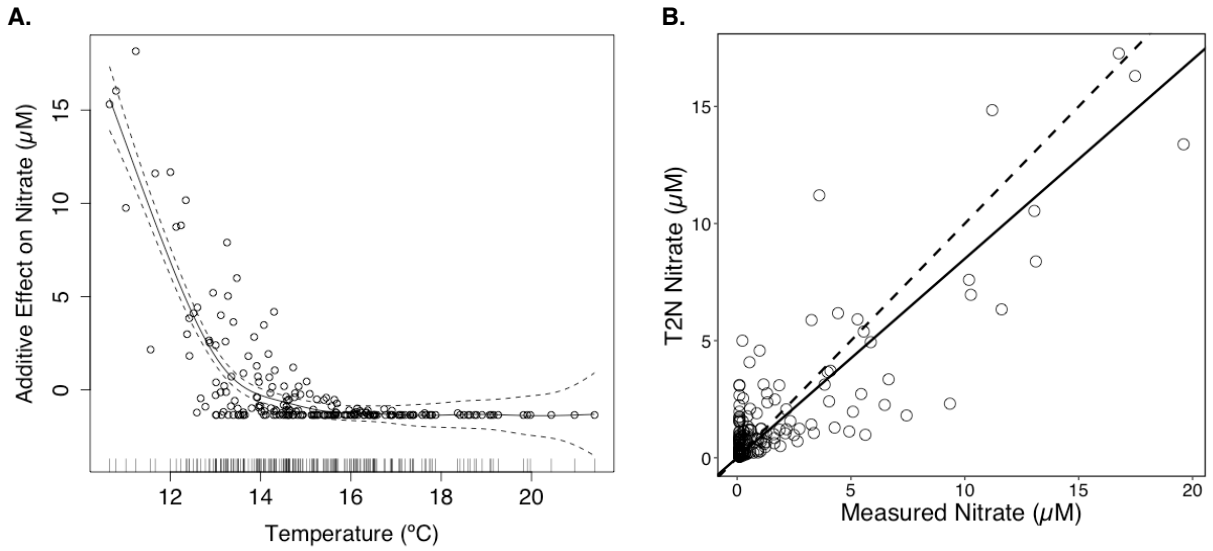

Figure S3: Temperature-to-nitrate (T2N) estimates. (A) Generalized additive model fit for the temperature to nitrate relationship at Mohawk Reef. The solid line is the model fit and the dashed lines show the standard error about the curve. Open circles show the *in situ* temperature and measured nitrate concentrations from 2006 to 2024. Vertical markings on the x-axis emphasize the density of observations along the temperature gradient. **(B)** Comparison between measured nitrate concentrations and the estimated nitrate concentrations from the T2N relationship. The dashed line is the 1:1 line and the solid line is the significant Model II linear regression (R^2 = 0.74; $p < 0.001$, n = 210, $y = 0.83x + 0.26$).

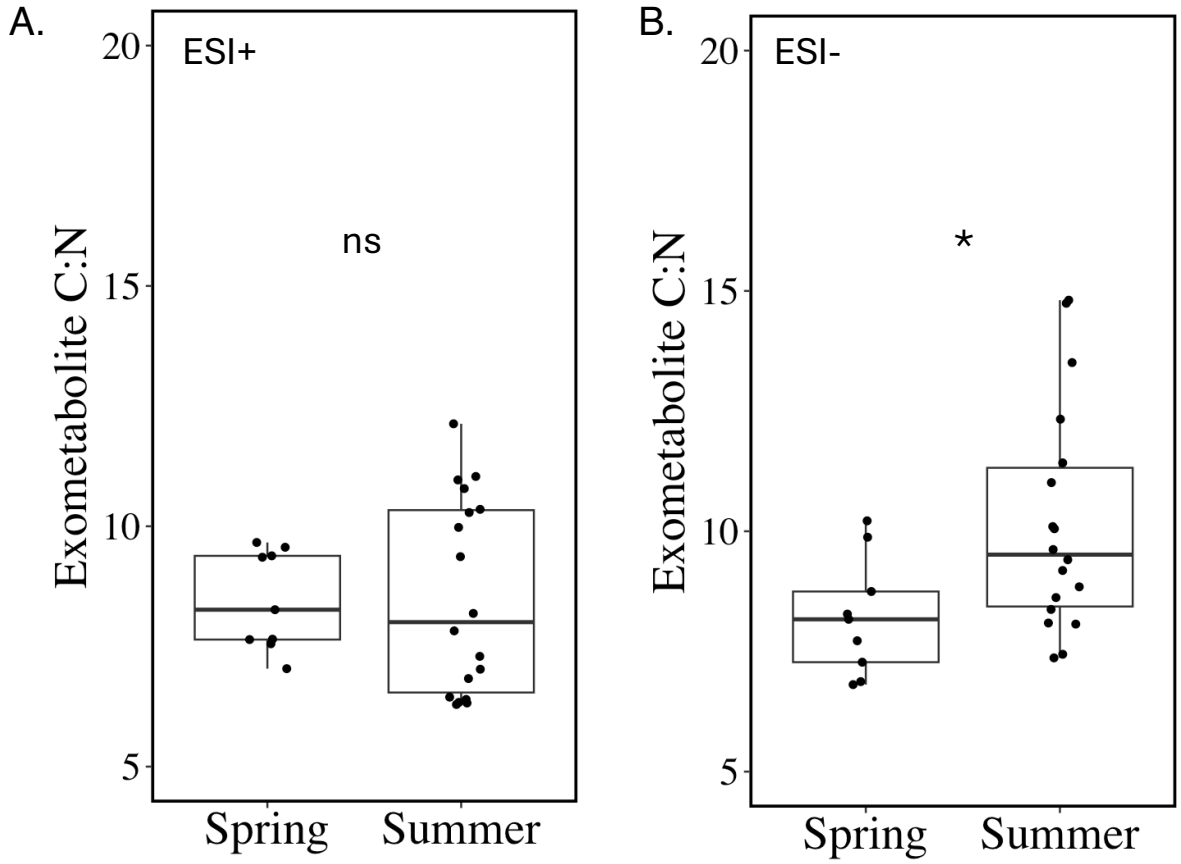

Figure S4: Mature developmental stage peak area weighted exudate carbon to nitrogen ratios (C:N) in **(A)** ESI+ and **(B)** ESI- modes. The ns and * indicate not significant and significant ($p < 0.05$) differences between the two seasons (Wilcoxon Rank test).

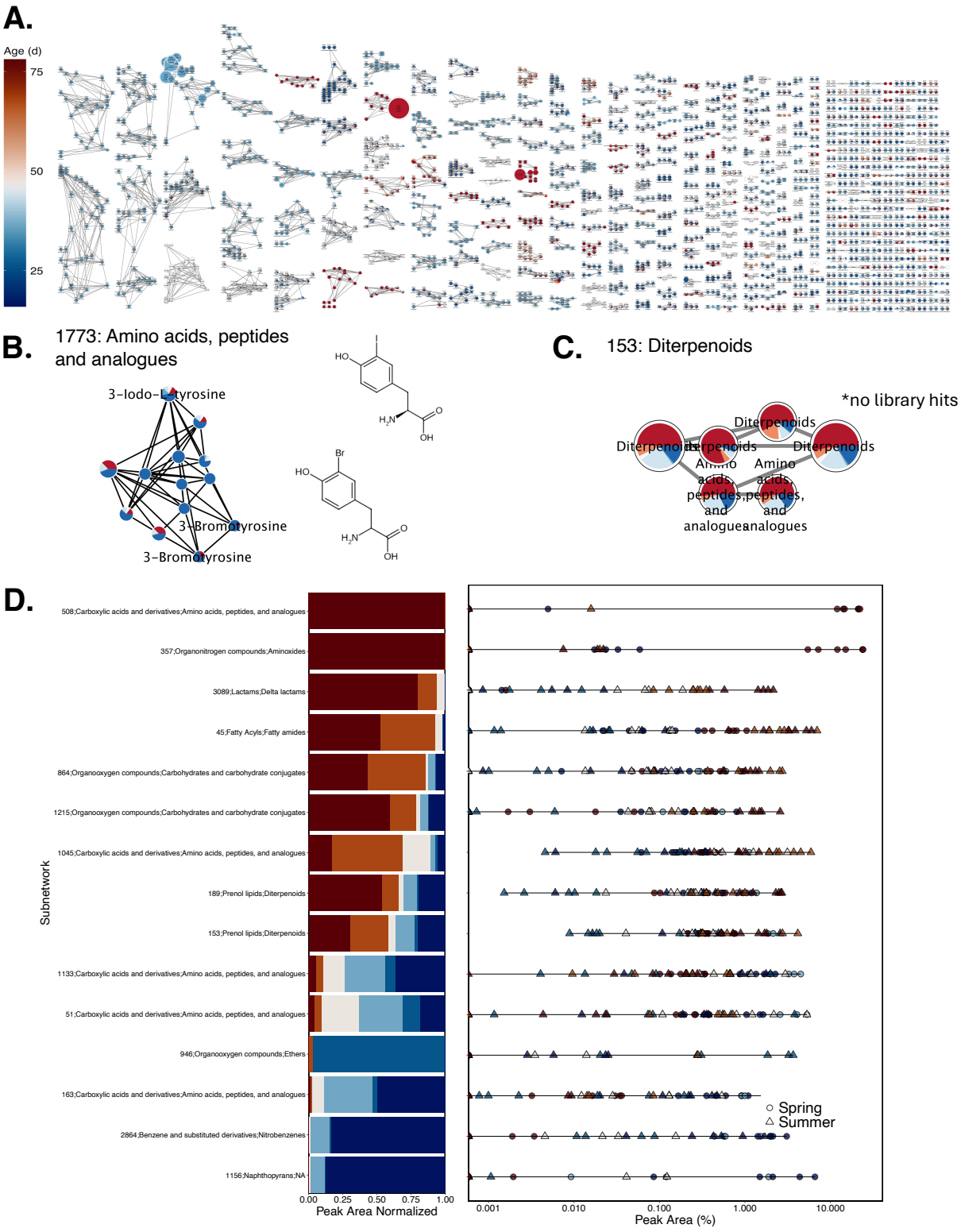
A.
Age (d)
75
50
25
B.
1773: Amino acids, peptides and analogues
3-Iodo-L-tyrosine
3-Bromotyrosine
3-Bromotyrosine
C.
153: Diterpenoids
*no library hits
Diterpenoids
Diterpenoids
Diterpenoids
Diterpenoids
Amino acids, peptides, and analogues
Amino acids, peptides, and analogues
D.
508;Carboxylic acids and derivatives;Amino acids, peptides, and analogues
357;Organonitrogen compounds;Aminoxides
3089;Lactams;Delta lactams
45;Fatty Acyls;Fatty amides
864;Organooxygen compounds;Carbohydrates and carbohydrate conjugates
1215;Organooxygen compounds;Carbohydrates and carbohydrate conjugates
1045;Carboxylic acids and derivatives;Amino acids, peptides, and analogues
189;Prenol lipids;Diterpenoids
153;Prenol lipids;Diterpenoids
1133;Carboxylic acids and derivatives;Amino acids, peptides, and analogues
51;Carboxylic acids and derivatives;Amino acids, peptides, and analogues
946;Organooxygen compounds;Ethers
163;Carboxylic acids and derivatives;Amino acids, peptides, and analogues
2864;Benzene and substituted derivatives;Nitrobenzenes
1156;Naphthopyrans;NA
Subnetwork
0.00
0.25
0.50
0.75
1.00
Peak Area Normalized
0.001
0.010
0.100
1.000
10.000
Peak Area (%)
Spring
Summer

Figure S5: **Distinct molecular feature subnetworks detected in ESI+ mode are significantly enriched across the developmental stage of giant kelp. (A)** Network of exudate features (nodes) linked by edges representing cosine similarity scores > 0.7 between nodes. Nodes are sized by the mean of the MS1 peak areas and colored by the mean proportion of the peak area at each age of the kelp. Representative FBMN subnetworks that are significantly enriched between developmental stages are shown in **(B)** and **(C)**. In **B**, structures and names of the spectral library matches are show. **(E)** The relative abundance of abundant subnetworks (mean peak area > 1%) with significantly different (Wilcoxon, FDR-adjusted $p < 0.05$) relative abundances between developmental stages. All subnetwork peak areas were normalized to 1 and the color shows the relative abundance of that subnetwork at different ages (16, 30, 37, 43, 64, 77 & 78 days). The corresponding point and line plot shows the range in subnetwork relative abundance across all samples in which the subnetwork was detected.

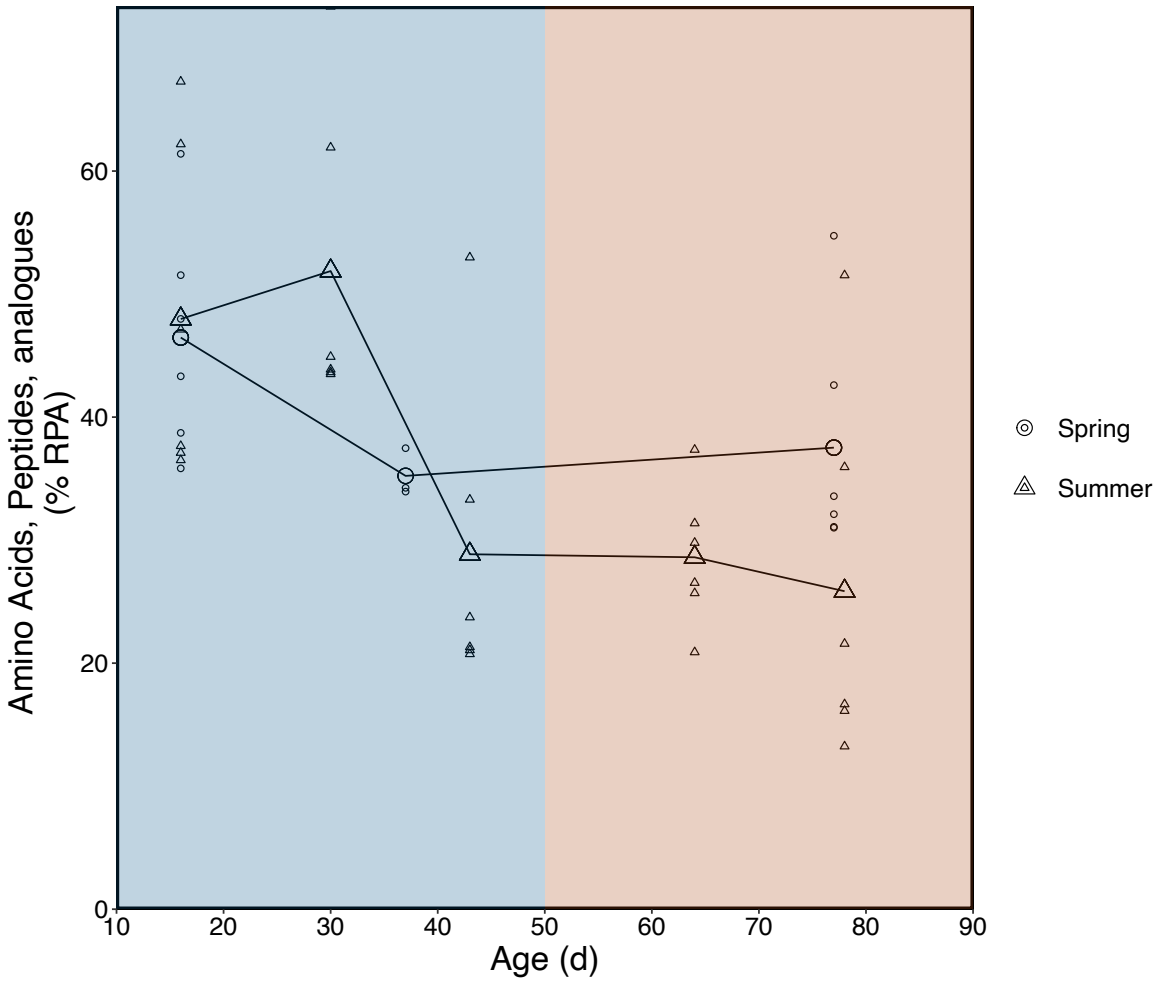

Figure S6: The relative abudnance of compound subclasses detected in positive mode (ESI+) across kelp age and between seasons classified as Amino acids, peptides, and analogues. Larger shapes indicate the mean value at each age and season and the smaller shapes represent the individual measurments.

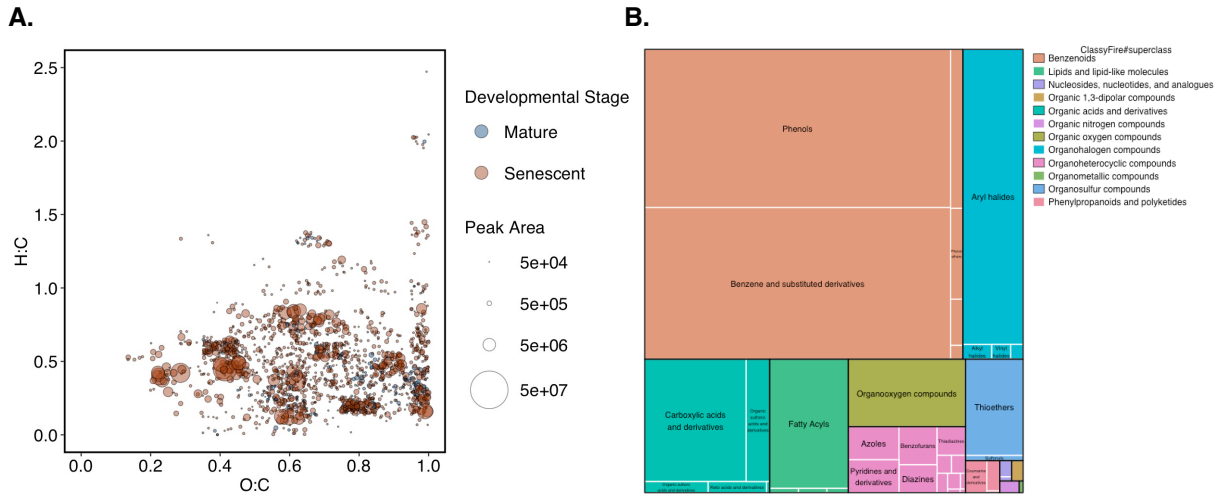

Figure S7: Chemical diversity of features containing bromine detected in ESI- mode. (A) Van Krevelen diagram showing the hydrogen to carbon (H:C) ratio versus the oxygen to carbon (O:C) ratios of bromine containing formulas (CHOBr) that were detected in either the mature and senescent developmental stages. **(B)** Tree plot of Classyfire super class (box color) and class annotations (inset text) of CHOBr features. The size of the boxes represents the relative peak area across all samples (n = 45).